Ecological interactions in breast cancer: Cell facilitation promotes growth and survival under drug pressure

Authors:

Rena Emond[1#], Jason I. Griffiths[1#], Vince Kornél Grolmusz[1#], Aritro Nath[1], Jinfeng Chen[1], Eric F. Medina[1], Rachel S. Sousa[2], Frederick R. Adler[3, 4*], Andrea H. Bild[1*]

Affiliations:

[1] Department of Medical Oncology and Therapeutics Research, Beckman Research Institute, City of Hope National Medical Center, Monrovia, CA

[2] Department of Mathematics, Oregon State University, Corvallis, OR, 97331

[3] School of Biological Sciences, University of Utah, Salt Lake City, UT, 84112

[4] Department of Mathematics, University of Utah, Salt Lake City, UT, 84112

# contributed equally

* To whom correspondence should be addressed:

Andrea H. Bild
City of Hope
1218 South 5th Avenue
Monrovia CA 91016
Email: abild@coh.org

Frederick R. Adler
201 Presidents Circle
Salt Lake City, UT 84112
Email: adler@math.utah.edu

Abstract

The interplay of positive and negative interactions between drug sensitive and resistant cells influences the effectiveness of treatment in heterogeneous cancer cell populations. In a study of isogenic estrogen receptor positive (ER+) breast cancer cell lineages sensitive and resistant to ribociclib-induced CDK4/6 inhibition in mono- and co-culture, we find that sensitive cells grow and compete more effectively in the absence of treatment. During treatment with ribociclib, sensitive cells survive and proliferate better when grown together with resistant cells than when grown in monoculture, termed facilitation in ecology. Both liquid chromatography-tandem mass spectrometry (LC-MS/MS) assays and single cell RNA-sequencing (scRNAseq) indicate that resistant cell production of estradiol, a highly active estrogen metabolite, is the mechanism of facilitation. Higher estradiol production by resistant cells drives a shift in sensitive cell phenotype to a resistant cell state in coculture. Adding estradiol in monoculture provides sensitive cells with increased resistance to therapy, and cancels facilitation in coculture. Mathematical modeling quantifies the strength of competition and facilitation and predicts that blocking facilitation has the potential to control both resistant and sensitive cell populations and inhibit the emergence of a refractory population.

Introduction

Breast cancer is the most common cancer worldwide and the second leading cause of cancer death in American women. The majority (~80%) of these breast tumors are estrogen receptor positive (ER+), and the majority of metastatic patients who die from their cancer have this breast cancer subtype (1-3). In these tumors, estrogen receptor activity leads to cancer cell proliferation through CDK4/6 activation and cell cycle progression (4-6). In order to target both upstream ER and downstream CDK4/6 signaling for cancer control, the combination of CDK inhibitors with endocrine therapy has been used successfully in metastatic ER+ breast cancer, and to a moderate extent in earlier-stage, non-metastatic breast cancer (7-12). However, tumors can develop resistance to both single and combination endocrine and cell cycle therapy regimens (7, 8, 10-15). Understanding the underlying causes of resistance to endocrine and cell cycle therapies is a critical area of research for this major cancer subtype and cause of death in women.

Cancerous tumors consist of genetically and phenotypically heterogeneous cells (16). Despite advancements in understanding tumor heterogeneity, this feature is not used in cancer treatment strategies. ER+ breast cancer is often polyclonal and phenotypically heterogeneous, with co-existing cells of different levels of estrogen receptor expression and different levels of estrogen addiction (17). Heterogenous tumors create three major obstacles for treatment. First, cells can have different susceptibilities to treatment, meaning that even a targeted treatment with high efficacy can fail to kill or inhibit a subset of cancer cells (18, 19). Second, this differential survival and proliferation can promote continued evolution of tumor resistance during drug therapy (16, 20). Third, heterogeneous cell populations create the possibility for interactions among cells which can alter responses to treatment and patient outcomes (21-27). In this case, understanding how subpopulations communicate could help design therapy strategies that disrupt and/or exploit these interactions for clinical benefit.

This study explores the dynamics of cell interactions, including cooperation and competition, in ER+ breast cancer. Cooperation takes multiple forms and seldom exists in isolation from competition (28, 29). We investigate **facilitation**, the widely-used ecological term describing cooperative cases where competitors of one type benefit those of another under appropriate conditions (30). For example, facilitation emerges among plants competing for water when one plant gains from water that leaks from the roots of a deeper-rooted neighbor (31). This coincidence of competitive and facilitative interactions requires detailed mathematical models to disentangle their concurrent effects, and experiments to identify mechanisms.

To investigate the type, strength and mechanism of cell interactions in heterogeneous cancer populations during treatment, we developed ER+ breast cancer cell lineages that are sensitive or resistant to CDK4/6 cell cycle inhibition (ribociclib), a standard therapy used to treat this cancer. Using mathematical models of population growth and interaction, we found that ribociclib resistant cells facilitate sensitive cancer cell growth during drug treatment. Experimental analysis using liquid chromatography-tandem mass spectrometry (LC-MS/MS) assays and Western blot analysis showed that resistant cells secrete estradiol, which given the sensitive cells' high dependence on estrogen for proliferation, leads to their growth promotion in coculture. Single-cell RNA-sequencing (scRNAseq) analysis revealed that during coculture sensitive cells acquire the traits of resistant cells and increase proliferation levels. Examining mono- and coculture growth trajectories across a broader range of drug doses, we parameterized a mechanistic model of facilitation. This

consumer-resource model revealed that facilitation impairs cell cycle inhibition therapy during the rapid cancer population growth phase and predicts that blocking facilitation can jointly control resistant and sensitive populations.

These studies uncover a novel mechanism of resistance in which increased levels of local estradiol, the active estrogen metabolite, is produced by a subset of cancer cells, leading to cooperative survival and growth of normally therapy-sensitive cells. By understanding cooperative interactions like facilitation, we have the potential to better control coexisting populations within a heterogenous tumor and inhibit the emergence of resistant phenotypes.

Results

Sensitive and resistant cell growth and treatment effects

We developed an *in vitro* model to study ER+ breast cancer cell interactions under selective drug pressure (see Methods). To generate isogenic lineages, we applied ribociclib to cell cultures for 6-9 months until resistance developed compared to control drug sensitive parental lineage not exposed to treatment (32). These resistant and sensitive lineages, derived from CAMA-1 ER+ breast cancer cell lines, were labeled with lentivirus to express a fluorescent protein for monitoring each population's growth when cocultured, and cell counts were calculated as a measure of spheroid area and fluorescence intensity integrated into fitted growth equations (**Supp. Fig. 1**). The procedure was repeated for two other cell lines, MCF7 and MCF7/LY2 (MCF7 cell line resistant to antiestrogen) (**Supp. Fig. 2**) (33, 34). When grown as 3D spheroids in monoculture, untreated sensitive CAMA-1 cell populations grew more quickly than resistant cells. In contrast, while under both 200nM and 400nM concentrations of ribociclib, resistant cells grew more quickly than sensitive cells **(Fig. 1a-b).** CAMA-1 sensitive cell proliferation was inhibited at higher ribociclib concentrations (200nM and 400nM) whereas resistant cell proliferation was inhibited much less **(Fig. 1c-d)**. The log fold change of the sensitive cell population between days 4 and 14 is reduced by a factor of 7.8 by 400nM ribociclib treatment, and that of the resistant cell population by a factor of 1.25. Similarly, MCF7/LY2 sensitive cell proliferation decreased with an increase in ribociclib treatment compared to resistant lineages (**Supp. Fig. 2**).

Ribociclib tolerance provided by facilitation of sensitive by resistant cells

To investigate whether cell interactions alter response to therapy, we compared growth of monocultured and cocultured sensitive and resistant cells treated with different doses of ribociclib over 18 days. We use Lotka-Volterra competition models (35) to quantify cell interactions and to predict the joint effect of treatment and coculture if one cell type does not alter the drug tolerance of the other. In particular, we determine the expected effect by estimating the cost of treatment and the cost of competition and predicting the combined effect by multiplying the reductions in the growth rate and the carrying capacity (**Supp. Fig. 8a** and Methods). This expected combined effect was then compared with observed growth. Observed growth greater than expected growth of sensitive cells in treated coculture indicates facilitation.

Using the competition model, we find that sensitive cells strongly suppress resistant cells in untreated cocultures, with a competitive effect 50% larger than that of resistant cells on themselves (scaled to 1.0 in these models). In contrast, resistant cells had almost no detectable competitive effect on sensitive cells (**Fig. 1e**). Facilitation was measured as the log observed growth relative to expected growth. Based on the individual effects of ribociclib and coculture, sensitive cells are expected to grow slightly more slowly in ribociclib treated coculture than in treated monoculture due to competition. Instead, we observed markedly increased growth showing facilitation of sensitive cells by resistant cells (facilitation under 200nM ribociclib = 0.973; facilitation under 400nM ribociclib = 2.39) (**Fig. 1f**). Reciprocally, resistant cells grew more slowly than expected in treated coculture due to the increased suppression by the sensitive cells they facilitate (facilitation under 200nM ribociclib = -0.055; facilitation under 400nM ribociclib = -0.227). Despite differences in competitive interactions, facilitation of sensitive cells was also observed in the additional ER+ cell lines, MCF7 (facilitation under 2.4uM ribociclib = 0.239; facilitation under 5uM = 0.4) and MCF7/LY2 (facilitation under 3uM = 0.659; facilitation under 5uM = 0.479), with MCF7/LY2 more closely resembling CAMA-1 cell growth and facilitation (**Supp. Fig. 2**).

Mechanisms of facilitation under ribociclib treatment

To determine the mechanisms driving facilitation during ribociclib treatment, we tested whether resistant cells metabolize ribociclib more effectively than sensitive cells, reducing the ribociclib concentration and allowing increased proliferation of cocultured sensitive cells. Using an optimized HPLC/MS method, we found that the ribociclib concentration was not decreased more in media incubated with resistant spheroids than with sensitive spheroids, and that ribociclib remained at high doses (**Supp. Fig. 3**).

Alternatively, ribociclib resistant cells may release signaling molecules that enhance the growth of sensitive cells under drug treatment. To test this hypothesis, we compared proliferation of sensitive cells when supplemented with conditioned media transferred from spheroids of different compositions (100% sensitive, 50%-50% sensitive/resistant, 100% resistant) with or without treatment (0 or 400nM ribociclib). Conditioned media originating from spheroids containing resistant cells increased proliferation of sensitive cells significantly more than conditioned media produced by sensitive cell spheroids, with the largest benefit from cells that were themselves treated **(Fig. 2a)**, indicating that resistant cells secrete signaling molecules that provide pro-growth benefits for sensitive cells under drug pressure. Comparisons of sensitive cell proliferation identified no effect of exosomal transfer on sensitive cell growth under treatment (**Supp. Fig. 4**).

To identify the molecules secreted by resistant cells that may promote growth under drug pressure, we measured the concentrations of a broad range of growth-promoting factors in the media of cultured spheroids. Custom multiplex cytokine analysis for detection of known growth factors (TGFβ 1-3, TGFα, EGF, and FGF2, FGF21, FGF23) showed no significant differences in levels in cocultured sensitive and resistant cells (**Supp. Fig. 5a and 5b**). However, concentration of estradiol, a potent estrogen compared to estrone, significantly differed between resistant and sensitive spheroids. We used liquid chromatography-tandem mass spectrometry (LC-MS/MS) assay to detect estrone (**Supp. Fig. 5c**) and estradiol concentration under no treatment or 200nM ribociclib treatment **(Fig. 2b)**. Estradiol was not detectable in media from 100% sensitive cell

195 cultures in either treatment; in contrast, samples from cultures containing resistant cells showed
196 measurable levels of 64 pg/mL. Estradiol production and uptake by resistant and sensitive cells
197 was estimated by fitting a Michaelis-Menten model (35) and accounting for limits of detection
198 (**Fig 2c, left panel, Supp. Inf.**). Resistant cells are estimated to produce approximately 8 times
199 more estradiol and use only 2.5 times more than sensitive cells **(Fig. 2c, right panel)**, generating
200 a substantial source of the growth-promoting hormone.

201 Given the higher estimation of estradiol produced by resistant cells, we investigated the estrogen
202 biosynthesis pathway and possible differences in the levels of enzymes involved in estradiol
203 metabolism between sensitive and resistant cells. In general, breast cancer cell lines express a
204 significantly lower level of estrogen synthetase, CYP19A1 (Aromatase), than non-cancer cell
205 lines, with ER+ breast cancer lines expressing much lower aromatase mRNA levels than ER- lines
206 (36, 37). However, differences in protein levels were detected in a subset of the core estradiol
207 metabolism conversion enzymesHSD17β1 (involved in the conversion of estrone to estradiol, the
208 more active estrogen metabolite), and HSD17β8 (an oxidative enzyme responsible for inactivating
209 estradiol) (**Fig. 2d)**. Western blot analysis of these conversion enzymes indicates higher detectable
210 levels of HSD17β1 in CAMA-1 resistant cells and higher levels of HSD17β8 in sensitive cells
211 (**Fig. 2d, Supp. Fig. 6**). Similarly, levels of HSD17β8 were found to be decreased in resistant
212 MCF7/LY2 and MCF7 cells (**Supp. Fig. 6**), suggesting that increased levels of estradiol may be
213 driven through multiple mechanisms. While MCF7/LY2, like CAMA-1, exhibited higher levels of
214 HSD17β1 in resistant cells, a distinction was not found between sensitive and resistant MCF7
215 cells, consistent with the lower facilitation in MCF7 cells than in MCF7/LY2 and CAMA-1.
216 Experiments in media deprived of androgens from charcoal stripped fetal bovine serum produced
217 total growth inhibition in both resistant and sensitive cells (**Supp. Fig. 7**). These analyses support
218 a model of facilitation whereby ribociclib resistant cells produce excess estradiol via an androgen
219 synthesis pathway with increased HSD17β1, countering sensitive cells' inactivation of estradiol
220 via HSD17β8, and ultimately promoting sensitive cell growth during treatment (**Fig. 2e**).

221 Applying ribociclib treatment in coculture reveals facilitation of sensitive cells by resistant cells.
222 Furthermore, the degree of facilitation increases in a dose dependent manner (**Fig. 3c**). Our
223 experiments indicate that resistant cells facilitate sensitive cells by increasing the level of local
224 estradiol. To test this mechanism, we added estrogen pathway modifiers to cells in monoculture
225 and coculture, both with and without ribociclib treatment, focusing on estradiol itself and the ER
226 antagonist fulvestrant, a selective estrogen receptor degrader (SERD). We measured strength of
227 facilitation in sensitive (**Fig. 3c, 3d**) and resistant cells (**Supp. Fig 8g, 8h**). We tested two specific
228 predictions.

229 1. *Facilitation will not be observed in cocultures treated with estradiol alone.*

230 Estradiol treatment alone improves the growth of sensitive cells in monoculture, consistent
231 with sensitive cells being more dependent on estradiol signaling. However, in coculture the
232 observed growth of sensitive cells is, in fact, slightly less than expected if the effects of
233 competition and estradiol were independent (**Fig. 3a, c, Supp. Fig. 8b**). This result supports
234 the hypothesis that without selective pressure, competition from sensitive cells blocks
235 resistant cell growth and facilitation of sensitive cells.

236 2. *Resistant cells will facilitate sensitive cells when treated with other agents that disrupt the*
237 *ER pathway, such as the ER antagonist, fulvestrant.*

238 In monoculture, cells resistant to ribociclib are also more resistant to fulvestrant, due to
239 their lower dependence on estrogen signaling. In coculture treated with fulvestrant,
240 resistant cells were found to facilitate sensitive cells, allowing them to proliferate more
241 than expected and enough to eventually outcompete resistant cells entirely (**Fig. 3b-c,**
242 **Supp. Fig. 8e**), with dose-dependent effects that parallel those with ribociclib.

243 Our hypothesis also makes two specific predictions about how facilitation is changed by addition
244 of estrogen pathway modifiers. To quantify these effects, we compare observed growth with a null
245 model that assumes that the effects of treatments are independent.

246 1. *Estradiol will cancel the facilitation of sensitive cells by resistant cells in the presence of*
247 *ribociclib.*

248 Addition of estradiol nearly cancels the facilitation of sensitive cells by resistant cells when
249 treated with ribociclib (**Fig. 3a, d, Supp. Fig. 8c, f**). We see no dose response likely due to
250 saturation of estradiol binding capacity of sensitive cells.

251 2. *Under ribociclib treatment, the addition of fulvestrant will strongly modify facilitation.*

252 When ribociclib is combined with fulvestrant, facilitation of sensitive cells is unchanged
253 at a low dose and increased at a higher dose (**Fig. 3b**), consistent with resistant cell
254 facilitation of sensitive cell growth under treatment by each of ribociclib and fulvestrant
255 separately (**Fig. 3d**).

256 Letrozole, an aromatase inhibitor (AI), only partially cancels facilitation, due to the existing
257 resistance of CAMA-1 cells (**Supp. Fig. 9a, b**). Other endocrine inhibitors, tamoxifen (**Supp. Fig.**
258 **9c, d**) and raloxifene (**Supp. Fig. 9e, f**), both selective estrogen receptor modulators (SERM),
259 completely cancel facilitation by disrupting the response of sensitive cells. The resulting degree of
260 facilitation modification between the treatment with a SERM or SERD is likely due to differences
261 in each inhibitor's mechanism of action. While both agent classes inhibit ER signaling, they do so
262 in different ways. SERMs bind to ER, resulting in an inactive complex, while SERDs disrupt
263 signaling by preventing dimerization and targeting ER for degradation. In our *in vitro* system, cells
264 resistant to ribociclib are also more resistant to the SERD, fulvestrant. However, SERMs are more
265 damaging to resistant cell growth while also blocking facilitation in sensitive cells as they directly
266 competing with estradiol at the receptor site, disallowing estradiol from binding to the receptor
267 which leads to the cancellation of facilitation.

268 **<u>Coculture results in a shift of sensitive cells to a more resistant cell state as revealed by</u>**
269 **<u>scRNAseq.</u>**

270 We hypothesized that hormone communications from resistant to sensitive cells activates
271 proliferative pathways of sensitive cells when cocultured during ribociclib treatment resulting in a
272 more resistant phenotype. We performed scRNAseq on sensitive and resistant CAMA-1 cells
273 grown in 3D after 11 days of treatment, both in monoculture and coculture with initially equal

274 proportions. Following quality control filtering and normalization of the scRNAseq profiles (see
275 **Methods**), we performed UMAP dimension reduction to compare the phenotypic similarity of
276 cells across the transcriptome. Monoculture sensitive and resistant lineages formed separate
277 clusters, indicating that they are phenotypically distinct, with a shift of sensitive cells towards
278 resistant cells seen when grown in coculture (**Fig. 4a**). We next calculated the cell cycle phase of
279 each cell using canonical markers (**Fig. 4b**) and found a striking increase in the proportion of
280 cycling sensitive cells in coculture compared to sensitive cells in monoculture. This analysis
281 revealed that resistant cells facilitated the cell cycle progression of sensitive cells under drug
282 pressure.

283 We next investigated the key pathway phenotypes acquired by the sensitive cells in coculture
284 compared to monoculture using single sample gene set enrichment analysis. We found a highly
285 significant increase in the KEGG and REACTOME cell cycle pathway enrichment scores (both
286 $p<0.00001$), supporting the cell cycle phase analysis results (**Fig. 4c**). Differential expression
287 analysis confirmed that both proliferation and estrogen signaling gene expression was elevated in
288 sensitive cells when cocultured compared to in monoculture (**Supp. Fig. 10**).

289 Gene expression signatures indicative estrogen signaling activation, including ESR1 targets ($p =$
290 3.1×10^{-111}) and estradiol response ($p=1.9 \times 10^{-153}$), were also elevated in sensitive coculture cells
291 (**Fig. 4d**). Finally, differential expression of estradiol production enzymes was detected between
292 resistant and sensitive cells with increased levels of HSD17β1 in resistant cells while HSD17β8
293 was elevated in sensitive cells (**Fig. 4e**), with low/non-detectable aromatase expression.

294 **<u>Measuring the impacts of growth factor mediated facilitation</u>**

295 To measure the impacts of estradiol mediated facilitation, we constructed stage-structured
296 consumer-resource differential equation models that describe the production and uptake of
297 estradiol, separate cell division and death, and include functional forms for the effects of ribociclib
298 and estradiol **(Fig. 5a)** (detailed in Methods and Supp. Inf.). We used Bayesian inference to fit the
299 model to the growth of monocultures and cocultures of sensitive and resistant cells across eight
300 doses of ribociclib.

301 The model of estradiol mediated facilitation accurately describes the growth of resistant, sensitive
302 and coculture spheroids across all drug doses **(Fig. 5b)** and additionally quantifies how biological
303 processes differed between resistant and sensitive cells **(Fig. 5c)**. Resistant cells were found to be
304 approximately 60% as competitive (α), consistent with the 1.5 times higher competitive effect of
305 sensitive cells (**Fig. 1f)**. Net production of estradiol (γ) by resistant cells was estimated to be
306 approximately twice that of sensitive cells, consistent with the ratio of production/use estimated
307 directly (8.0/2.5 = 3.2, **Fig. 2c**). In the absence of treatment, the less competitive resistant cells had
308 a baseline division rate (r) 50% of sensitive cells and a lower quiescence rate (λ). However, they
309 were far less sensitive to the cell cycle inhibitory effects of ribociclib (k), allowing their spheroids
310 to continue to grow at high doses.

311 We verified that models of alternative mechanisms of cell interaction could not produce the
312 diversity of spheroid growth trajectories observed across drug doses and compositions. Alternative

313 models included direct competition for resources and phenotypic plasticity in which cells transition
314 from a naive to a resistant state either in response to drug induction or via random switching
315 (detailed model comparisons provided in Supp. Inf.). We performed formal probabilistic model
316 comparison of the non-nested set of model hypotheses using Watanabe–Akaike information
317 criterion (WAIC). The facilitation model greatly outperformed models of competition or
318 phenotypic plasticity (**Supp. Fig. 11)**. This analysis guarded against model overfitting and supports
319 the estradiol mediated facilitation hypothesis.

320 We used the estradiol mediated facilitation model to explore the impact of therapeutically blocking
321 facilitation on the growth of sensitive and resistant co-cultured populations. In the model, we
322 reduced the binding of estradiol to its cellular receptor (μ) by differing degrees to reflect exposure
323 to different doses of a receptor blocking drug such as fulvestrant. In the absence of facilitation
324 blocking, the facilitation model accurately predicts the final resistant and sensitive cell population
325 size (**Fig. 5d**; points show observed final cell counts at day 21, black line + yellow overlay shows
326 model predictions under the experimental conditions). However, facilitation needed to be reduced
327 by more than 50% before substantial reductions in spheroid growth were predicted, suggesting that
328 resistant cells produce sufficiently large amounts of estradiol to saturate the growth benefits of
329 facilitation. At lower ribociclib doses (<500nM), facilitation blocking caused a more severe
330 reduction in the abundance of sensitive than resistant cells, suggesting that resistance could be
331 promoted under these circumstances.

332 Finally, we assessed the importance of facilitation relative to resource competition in determining
333 the rate of spheroid growth throughout treatment **(Fig. 5e)**. Across ribociclib doses (<600nM) we
334 showed that facilitation was many times more important than competition during the period after
335 the accumulation of a sufficient population size to generate high levels of estradiol but prior to the
336 spheroid reaching maximal density and becoming regulated by resource limitation. At moderate
337 ribociclib doses (200-600nM), the facilitation window shifts later into the treatment, as resistant
338 cell abundances increase more slowly, and the window also extends for a longer duration. At the
339 highest ribociclib doses (>600nM), the window of facilitation closes completely because
340 proliferation of resistant facilitating cells is controlled (shown in **Fig. 5e**). Coculture spheroid size
341 then shrinks during treatment as the small resistant population alone cannot maintain estradiol
342 levels to overcome treatment.

343 Discussion

344 We developed *in vitro* model systems to investigate how interactions between cancer lineages
345 impact the growth of heterogeneous ER+ breast cancer populations. We found that cells sensitive
346 to ribociclib (CDK 4/6 cell cycle inhibitor) grow faster in untreated monoculture and outcompete
347 resistant cells in coculture. However, in the presence of ribociclib, resistant cells facilitate the
348 growth of sensitive cells by producing estradiol, a potent estrogen metabolite, and upregulation of
349 estrogen signaling and proliferation. Although resistant cells were developed by long-term growth
350 with ribociclib, they also acquired cross-resistance to endocrine therapy due to a common signaling
351 pathway and thus also facilitate growth of sensitive cell populations in the presence of ER

antagonists. These patterns of cross-resistance and cell-cell interactions complicate patient treatment even beyond the challenge of evolution of resistance.

We use mathematical models to quantify competitive and facilitative interactions, and to predict how different conditions will alter facilitation. Mathematical models that include facilitation improve our ability to describe the growth of heterogeneous cancer populations. These models predict that blocking facilitation has the potential to control both resistant and sensitive cell populations and inhibit the emergence of a refractory population, prolonging the benefits of ribociclib. This may explain why ribociclib is more effective when combined with antiestrogen therapy than as monotherapy for some patients (38-40).

Our dynamical models highlight that the contribution of facilitation to proliferation and cancer population growth shifts during the growth of the cancer. As cell abundance increases, facilitation-driven growth diminishes as carrying capacity is reached, due to an increase in resource competition. This shift suggests that competitive ability may be more essential at later stages in disease progression, while facilitation may be more important in earlier stages. Future studies may also integrate local spatial effects in our measurements and modeling to account for any impact in cell-cell interactions.

Mathematical modeling (41-43) and experimental (44-46) research proposes that tumor growth and progression may be promoted by cooperation among diverse cell populations by sharing of resources or products through mechanisms including neoangiogenesis (41) and growth factor production (46). Our results support the concept that cancer cell facilitation may impact heterogeneous tumor growth during treatment in ER-positive breast cancer. No current therapy is directed specifically at cooperative cancer cell interactions. However, as tumors are often comprised of multiple subclonal populations, interactions between cells may provide targets for long-term treatment strategies. Given that facilitation can increase both persistence and biomass relative to simpler systems with resource competition only (47, 48), it is likely to be frequent in heterogeneous cancer populations. As we gain in capabilities to measure the growth of heterogeneous subclone populations during treatment, we may tailor strategies to control faster growing yet drug sensitive cells while preventing dominance of refractory cells through competition with more fit subclones.

This study describes facilitation through an increase of local estradiol concentrations by resistant cells that stimulates proliferation of sensitive cells during selective pressure. It is known that estrogen biosynthesis and metabolism can be upregulated in cancer cells (49-51). It remains unknown whether resistant cells in our system acquired mutations to increase estradiol levels or if changes are epigenetic. The increase of active estrogen is important given that the majority of breast cancers are hormone receptor positive, and resistance to first line standard of care hormone therapy is common (52-54). In patients with increased levels of estradiol, potential treatment strategies include blocking the enzymes that synthesize estradiol in resistant cells or modulating the level or type of endocrine therapy given to a patient. Targeting the diffusible facilitation factor has been proposed to be a more evolutionarily stable treatment strategy than targeting the cancer cell receptors or signaling pathways (55) because the production provides little benefit to the producing cell. An important next step is to study these mechanisms in patient tumors, and to better understand the presence and impact of cell cooperation in response to therapy and outcomes.

396 In conclusion, our data indicate that the facilitation within heterogeneous cancer cell populations
397 shapes the dynamics of resistance and cancer growth of the population as a whole. We show that
398 local production of a highly active estrogen, estradiol, facilitates the growth of sensitive cells in
399 the presence of drug treatment, is produced by resistant cells, and conveys resistance to anti-
400 proliferative effects of cell cycle inhibition in sensitive cells. We use mathematical models to
401 measure these processes and show that blocking this facilitation could promote response of the
402 entire cancer population, reducing selection for refractory resistant states. This work provides
403 support for the development of strategies to modulate facilitation to create robust and durable
404 cancer control.
405

406 # Methods

407 ## *Cell lines and reagents*

408 The previously authenticated estrogen-receptor-positive (ER+) CAMA-1 breast cancer cell lines
409 were maintained in DMEM+ 10% FBS+ 1% antibiotic–antimycotic solution. The ribociclib-
410 resistant CAMA-1 cell line creation (ribociclib-resistant CAMA-1) was previously reported (32).
411 Briefly, cells were cultured and continuously treated with ribociclib (Selleck Chemicals, Cat. No:
412 S7440) at 1μM for 1 month. Following the initial 1μM ribociclib treatment, cells were treated with
413 250nM for 4 months to develop resistance. Maintenance of ribociclib-resistant CAMA-1 cells
414 continued in complete culture medium + 250 nM ribociclib. Resistance against ribociclib was
415 detected by the alteration of the dose–response curve measured using CellTiterGlo
416 Chemiluminescent Kit (Promega Corporation, Cat. No.: G7573).

417 ## *Lentiviral labeling of sensitive and resistant cells*

418 Using lentiviruses incorporating distinct fluorescent proteins, we labeled CAMA-1 parental
419 sensitive cells (venus; LeGO-V2) and ribociclib resistant cells (cerulean; LeGO-Cer2). LeGO-V2
420 and LeGO-Cer2 vectors were provided by Boris Fehse (Addgene plasmids #27340 and #27338).
421 Lentiviruses with fluorescent proteins were created using Lipofectamine 3000 reagent (Thermo
422 Fisher Scientific) following manufacturer's protocol. CAMA-1 sensitive and resistant cell lines
423 were transduced with lentivirus using reverse transduction. Briefly, 1mL of polybrene-containing
424 cell suspension of 200,000 cells were plated in a well of a 6-well plate. Previously, 0.5 mL of viral
425 aliquot had been dispensed in plate. Following 48 hours of incubation at 37 ºC with 5% CO_2, cells
426 were washed and given fresh regular culture medium. To select for fluorescence-activated cells,
427 fluorescently labeled cells were flow-sorted after further subculture of transduced cells attain
428 homogenously labeled cell populations.

429 ## *Mono- and coculture 3D spheroid experiments*

430 18-21 day-long experiments were initiated with fluorescently labeled sensitive and resistant cell
431 lines in different compositions. For CAMA-1 spheroid experiments, as earlier reported (32), 2000
432 cells were plated in different proportions (100% CAMA-1 sensitive, 50% CAMA-1 sensitive—
433 50% CAMA-1 resistant, 100% CAMA-1 resistant) in 96-well round-bottom ultra-low attachment
434 spheroid microplate (Corning, Cat. No.: 4520). 24 h later, spheroids were washed and fresh
435 medium including treatment drugs was applied. Spheroids were treated for a total of 18-21 days

436 with imaging and media change performed at every 4th and 7th day of the week. Spheroids were
437 treated with the following drug therapies at specified doses described in results and figures 1 and
438 4: ribociclib (Selleck Chemicals, Cat. No: S7440), estradiol (Peprotech, Cat. No: 5022822),
439 fulvestrant (Selleck Chemicals, Cat. No: S1191). Imaging was performed using Cytation 5 imager
440 (Biotek Instruments) recording signal intensity from brightfield, YFP (for Venus fluorescence)
441 and CFP 450/440 (for Cerulean fluorescence) channels. Raw data processing and image analysis
442 were performed using Gen5 3.05 and 3.10 software (Biotek Instruments). Briefly, the stitching of
443 2 × 2 montage images and Z-projection of 6 layers using focus stacking was performed on raw
444 images followed by spheroid area analysis. To quantify growth under these conditions, we
445 measured fluorescence intensity and growth of spheroid area over the total time of the experiment.
446 For cell count calculations, a standard curve was created by measuring the area of spheroids after
447 plating at different cell numbers 24 hours after plating. A resulting equation by fitting a curve to
448 the data was performed by GraphPad Prism 7.02 software (second order polynomial – quadratic –
449 curve fit used). Whole spheroid area and fluorescence intensity measurements of each population
450 were integrated into the fitted equation, and cell counts for each population were produced from
451 fluorescence intensities relative to spheroid size. All coculture experiments were performed in
452 triplicates.

453 ***<u>Cell number quantification</u>***

454 For CAMA-1 cells, cell numbers were quantified as described previously (Grolmusz et al, 2020).
455 In brief, the relationship of area to cell counts follows a nonlinear curve (**Supp. Fig. 1a**), and
456 sensitive and resistant CAMA-1 cells have similar relationships of area to fluorescence (**Supp.**
457 **Fig. 1b**). Cell numbers were estimated by inverting the non-linear function, with proportions of
458 the two cell types estimated by the normalized relative fluorescence of each wavelength.

459 To estimate cell numbers for MCF7/LY2 cells, we measured cell numbers and spheroid area for a
460 range of initial fractions of sensitive (S) and resistant (R) cells and fit to a Michaelis-Menten
461 function maximum value A and half-saturation constant K (**Supp. Fig. 1c**). The relationship
462 differs depending on the proportion of S cells. Parameters are $K=2.753x10^5$, $A=1.094x10^7$ with
463 pure R cells and $K=2.119x10^5$ and $A=5.459x10^6$ with pure S cells, and $K=2.330x10^5$ and
464 A=7.546e6 $x10^5$ with mixed cultures (the dashed red curve).

465 To correct for possible differences in per cell fluorescence, we regressed the fluorescence of pure
466 cultures against the known numbers of S and R cells (**Supp. Fig. 1d**). We find a slope of 8.04
467 $x10^4$ for S cells and $1.349x10^5$ for R cells, and thus estimate that each R cell produces 1.677 times
468 as much fluorescence. To find the numbers of S and R cells in coculture from the area and the
469 fluorescence, we find the total cells by inverting the relationship between cells and area, and the
470 proportion of each cell type from the fraction of fluorescence, with R cells reduced by the
471 weighting factor of 1.677.

472 To estimate cell numbers for MCF7 cells, we followed the same procedure, finding Michaelis-
473 Menten fits (**Supp. Fig. 1e**) with parameters $K=1.772x10^5$, $A=9.061x10^6$ with pure R cells and
474 $K=5.315x10^5$ and $A=1.138x10^7$ when there are any S cells in the culture. We correct for

fluorescence in the same way (**Supp. Fig. 1f**), finding a slope of 8.36×10^4 for S cells and 2.029×10^5 for R cells, and thus estimate that each R cell produces 2.426 times as much fluorescence.

<u>Liquid chromatography-tandem mass spectrometry (LC-MS/MS)</u>

Media samples taken at day 21 from 3D spheroid experiments, treated with or without ribociclib, (experimental setup previously described in results and methods - ***Mono- and coculture 3D spheroid experiments***) and plated in different compositions (100% sensitive, 50% sensitive – 50% resistant, and 100% resistant) were spun down at 300g and frozen at -80 ºC. Samples were then prepared by the Analytical Pharmacology Core of City of Hope National Medical Center for LC-MS/MS for estrone and estradiol detection. LC-MS/MS system consisted of a Shimadzu Prominence HPLC system interfaced to an AB SCIEX QTRAP® 5500 system (Foster City, CA, USA). HPLC separation was achieved using a XSELECT CSH Phenyl-Hexyl 3.5um, 2.1x150mm analytical column (Waters). The column temperature was maintained at 50ºC, and the flow rate was 0.38ml/min. The mobile phase consisted of A (Water: 1000ml + 60ul 30%NH4OH) and B (Methanol : 1000ml+ 60ul 30% NH4OH). The following gradient program was used: 55% B (0.01 min), 70% B (0.01-4.0 min), 100% B (5.5min), 30%B (8.5min). The total run time was 8.5min. The auto-injector temperature was maintained at 15ºC. The atmospheric pressure chemical ionization (APCI) source of the mass spectrometer was operated in negative ion mode with ion source gas (55), curtain gas (20), collision gas (High), nebulizer current -4.0, The entrance potential was set to -10V. Declustering potential (DP) was -110, collision energy (CE), and collision cell exit potential (CXP) was optimized to -50V, -21V for Estrone, -160V, -50V,-17V for Estrone internal standard), -210V,-58V,-19V for Estradiol and -205V,-52V, -13V for Estradiol internal standard respectively. The source temperature was 400 ºC. A solvent delay program was used from 0 to 3.5 min and from 6.5 to 8.5min to minimize the mobile phase flow to the source. Analyst software version 1.5.1 was used for data acquisition and processing. Atmospheric – pressure chemical ionization of Estrone, Estrone D4, Estradiol, Estradiol D5 produced abundant protonated molecular ions (MH-) at m/z 268.980, 272.983, 270.969, and 275.981 respectively. Fragmentation of these compounds was induced under collision induced dissociation conditions. The precursor→product ion combinations at m/z 268.980→145.200 for Estrone, and 272.983→147.100 for Estrone-I.S. 270.969→182.800 and 275.981→147.000 for Estradiol and Estradiol-IS were used in multiple-reaction monitoring mode for quantitation. Under optimized assay conditions, the retention times for Estrone, Estrone IS and Estradiol, Estradiol -IS. were 4.89, 4.60 min, respectively.

<u>Single cell RNA Sequencing</u>

Spheroids of different compositions (100% sensitive, 50% sensitive – 50% resistant, 100% resistant) were initiated from Venus-labeled and mCherry-labeled CAMA-1_ribociclib_resistant cells and were subjected to 1 uM ribociclib treatment. After 11 days, spheroids were harvested, washed and cell suspensions were viably frozen for further processing. Once thawed, cells were centrifuged at 300 x g and washed twice with 37°C pre-warmed 1x PBS, pH 7.4 (Gibco, Cat #10010) + 0.04% Nuclease-Free Bovine Serum Albumin (BSA, EMD Millipore, Cat # 12661525mL). Cells were resuspended to a target concentration of 1,000 cell/µL, concentrations were confirmed using trypan blue staining and counted on a hemocytometer. scRNA-Seq was

516 performed on resuspended cells using the 10X Genomics Chromium Single Cell 3' GEM, Library,
517 & Gel Bead Kit v3 (10X Genomics, Cat # 1000075) according to manufacturer instructions at a
518 target of 10,000 cells per sample. Each sample was barcoded with a unique i7 Index during library
519 preparation using the Chromium i7 Multiplex Kit (10X Genomics, Cat# 120262) to allow sample
520 multiplexing during sequencing. Libraries were sequenced at Fulgent Genetics, on an Illumina
521 HiSeq X Ten instrument with 2x150 paired end reads, to a read depth of 10,000 reads per cell;
522 additional sequencing was performed on an Illumina NovaSeq 6000 with 2x150 paired end reads
523 increase read depth to a total depth of 50,000 reads per cell.

524 ***Single Cell Analysis***

525 scRNA-Seq was performed at the Integrative Genomics Core at City of Hope, Fulgent Genetics,
526 and the High Throughput Genomics Core at Huntsman Cancer Institute (HCI) of University of
527 Utah. Sequence reads were processed with CellRanger v3.0.2 using reference genome (GRChg37).
528 A gene-barcode matrix was generated for each sample containing counts of unique molecular
529 identifiers (UMIs) for each gene in each barcode (cell). The matrix was processed with Seurat
530 v3.1.1.9023 (56) to identify cell populations. A series of filters were applied to the data before
531 performing clustering. First, high-quality cells were retained by using the following filters in
532 Seurat: subset = nFeature_RNA < 7000 & nFeature_RNA > 3000 & nCount_RNA > 2000 &
533 nCount_RNA < 60000 & percent.mt < 30. Second, doublet cells were predicted with scrublet
534 (threshold=0.25) (57) and the predicted doublets were removed from further analysis. Third, cells
535 expressing mCherry or mVenus were retained by using cells having 2 or more UMI counts of
536 either mCherry or mVenus. The filtered UMI count matrix was normalized with method
537 "LogNormalize" and "scale.factor=10000". The top variable 2000 genes were identified and were
538 used to perform Principal component analysis (PCA) and clustering in Seurat. Cell clusters were
539 visualized using Uniform Manifold Approximation and Projection (UMAP). Differential
540 expressed genes between cell populations were identified using MAST (58) as implemented in
541 Seurat using FindMarkers function (abs(foldchange) >= 0.2 & Adjust P value <= 0.05). Genes
542 were ranked based on fold change. Pathway analyses were performed on 50 hallmark signatures
543 (MSigDB, hallmark) (59) and 4725 curated pathway signatures (MSigDB, c2) using single
544 samples gene set enrichment analysis implemented in the R package GSVA (60). Significant
545 differential pathway activity was identified using Wilcox rank sum test.

546 ***Western blot analysis of CAMA-1 cells***

547 Lysates of CAMA-1 cells were separated by SDS-polyacrylamide gel electrophoresis and proteins
548 were transferred electrophoretically to a polyvinylidene difluoride membrane using Invitrogen
549 iBlot 2 device and Invitrogen iBlot Transfer Stacks. Membranes were blocked with Tris-buffered
550 saline with 0.05% tween 20 (TTBS) and 5% BSA for 1 hour at room temperature. After washing
551 with TTBS, membranes were then probed with anti-HSD17β1 polyclonal antibody (Abnova,
552 H00003292-M03A, 1:1000 dilution, overnight 4°C; R&D systems, MAB7178, 1:2000 dilution,
553 overnight 4°C), anti-HSD17β8 polyclonal antibody (Proteintech, 16752-1-AP, 1:1000 dilution,
554 overnight 4°C), and anti-β-actin monoclonal antibody (Santa Cruz Biotechnology, sc-47778, 1:500
555 dilution, 1 hour room temperature) and detected using SuperSignal West Pico PLUS
556 Chemiluminescent Substrate (Thermo Scientific) with anti-rabbit (GE Healthcare NA9341ML) or

anti-mouse (GE Healthcare NXA9311ML) peroxidase-linked secondary antibody (1:6000 dilution). The molecular weight was determined using a pre-stained protein marker (BioRad).

Estradiol production and uptake analysis

To estimate the production and use of estradiol by sensitive and resistant cells, we compare the fits of three functions, each based on Michaelis-Menten kinetics by minimizing the least squares difference from the observed estradiol concentration. The full model includes separate production and uptake rates for each cell type. We estimate the production parameters ρ_R and ρ_S and the uptake parameters a_R and a_S, where R and S represent the measured cell numbers, with the function:

$$f_4 = \frac{\rho_R R + \rho_S S}{1 + a_R R + a_S S}$$

We examined simpler models that restrict the values. To test a model without production by sensitive cells, we set $\rho_S = 0$, giving:

$$f_3 = \frac{\rho_R R}{1 + a_R R + a_S S}.$$

Because uptake by cells is large compared with background usage (scaled to 1 in each of these models), we tested a simplified model with background usage set to zero. Without that term, the model is overparameterized, and we scale $a_R = 1$. In this case, a_S represents per cell uptake by sensitive cells relative to resistant cells, and the function simplifies to:

$$f_2 = \frac{\rho_R R + \rho_S S}{R + a_S S}.$$

During model fitting, we eliminated one outlier (Sample F8). We used the reported lower limit of detection of LLOD = 62.5 and set all measured values of 0 to LLOD/2. Neglecting this adjustment leads to significantly worse fits.

Model f_3 provided a poor fit. The best fit with model f_4 estimates $\rho_R = 83.58,\ \rho_S = 10.11, a_R = 0.864, a_S = 0.345$ and a residual sum of squares of 7321.1. The best fit parameters with model f_2 have the same residual sum of squares, with estimates $\rho_R = 96.79, \rho_S = 11.71, a_S = 0.400$. Due to the equally good fit with one fewer parameter, we choose this as our final model.

To find confidence limits, we use the residual sum of squares to estimate the variance and convert the least squares into a likelihood. We find values of each parameter with log likelihood within 2 of the maximum. With model f_2, we find limits $\rho_R \in [91.49,102.08], \rho_S \in [9.88,13.54],\ a_S \in [0.355,0.460]$.

Mathematical modeling – FACT analysis

Facilitation Analysis through Combination Therapy: The FACT algorithm breaks into six steps, which we outline here before describing in detail below. Modifiers refer to estrogen pathway modifying treatments, including estradiol itself and three ER antagonists: fulvestrant, tamoxifen,

and raloxifene.

1. **Fit growth and carrying capacity** for each cell type in monoculture with no treatment.
2. **Treatment effects:** Using the carrying capacity in the absence of treatment, find the effects of ribociclib or modifier treatment on cell growth and death rates.
3. **Synergy:** From growth with combined ribociclib and modifier treatment, compare observed growth with that expected under a null model without interaction.
4. **Competitive effect:** Using the carrying capacities and growth in sensitive and resistant cells in monoculture from Step 1, estimate competition coefficients between the two cell types in coculture.
5. **Facilitation:** Using the carrying capacities, growth and death rates of single cell types with or without ribociclib from Steps 1 and 2, and the competition coefficients in the absence of treatment from Step 3, quantify facilitation as deviations of growth from predicted under a null model. To quantify facilitation in the presence of modifier we follow the same steps but with modifier treatment.
6. **Facilitation modification:** Using the growth of cells in competition with ribociclib (Step 5) and the direct effects of modifier (Step 2), quantify whether the modifier enhances or reduces facilitation.

Mathematical methods

We fit each model with least squares, using all three replicates and the observed mean on day 4 for the initial condition. We exclude the measurements before day 4 because the cells often show a lag before beginning their growth.

1. Fit growth and carrying capacity to single cell data in the absence of treatment. We use the logistic model, as defined by the differential equations for sensitive and resistant cells

$$\frac{dS}{dt} = r_S\left(1 - \frac{S}{K_S}\right)$$

$$\frac{dR}{dt} = r_R\left(1 - \frac{R}{K_R}\right)$$

Equation (1)

to estimate r_S, r_R, K_S and K_R as the growth rates and carrying capacities of sensitive (S) cells and resistant (R) cells.

2. Treatment and modifier effects: Using the carrying capacity in the absence of treatment we estimate growth with treatment (r_{ST} , r_{RT}) as shown, and with modifier (r_{SM} , r_{RM}) with the model

$$\frac{dS}{dt} = r_{ST}\left(1 - \frac{S}{K_S}\right)$$

$$\frac{dR}{dt} = r_{RT}\left(1 - \frac{R}{K_R}\right)$$

Equation (2)

3. Synergy: To quantify how ribociclib interacts with modifiers in monoculture, we fit the logistic model using carrying capacities from Step 1, and compare the estimated growth r_C with the null

model:

$$r_S\left(\frac{r_{ST}}{r_S}\right)\left(\frac{r_{SM}}{r_S}\right)$$

Equation (3)

4. Estimate competition coefficients: Using the estimates of the growth rates and carrying capacities from Step 1, we fit untreated coculture data to a Lotka-Volterra competition model with competition coefficients α_{SR} and α_{RS}

$$\frac{dS}{dt} = r_S\left(1 - \frac{S + \alpha_{SR}R}{K_S}\right)$$

$$\frac{dR}{dt} = r_R\left(1 - \frac{\alpha_{RS}S + R}{K_S}\right)$$

Equation (4)

5. Estimate facilitation: We estimate facilitation as the deviation between observed and expected growth. To find expected growth, we use the estimates of the growth rates in monoculture with treatment, carrying capacities from the untreated monoculture, and the competition coefficients from the untreated cocultures.

6. Facilitation modification: If the presence of the other cell type enhances growth in the presence of ribociclib, a modifier could cancel or enhance this effect. To quantify, we use the growth parameter from step 4 in the presence of ribociclib, and account for the direct effects of the modifier as in step 2.

<u>Facilitation Analysis by Combination Therapy – Mechanistic model:</u>

Facilitation factor production, flux and utilization

To describe the mechanisms of facilitation between resistant (R) and sensitive (S) cells, we model the intracellular concentration of the facilitation factor (E) in each cell type (E_S, E_R) and the flux of this factor between cell types via the shared extra-cellular environment (E_E). We describe the intracellular production of this factor by sensitive and resistant cells at rate ρ_S and ρ_R and the receptor binding for utilization as a growth promoting signal at rate μ_S and μ_R. Facilitation factors diffuse between cells types and the extra-cellular environment at rate η. Finally, we describe the influx (σ_E) and decay (δ_E) of facilitation factors from the external environment. This leads to the following set of differential equations describing cellular and environmental concentrations of facilitation factors:

$$\frac{dE_S}{dt} = \rho_S + \eta(E_E - E_S) - \mu_S E_S$$

$$\frac{dE_R}{dt} = \rho_R + \eta(E_E - E_R) - \mu_R E_R$$

$$\frac{dE_E}{dt} = \sigma_E + \eta(E_S - E_E) + \eta(E_R - E_E) - \delta_E E_{E.}$$

Equation (5)

The equilibrium of this system is:

$$E_E^* = \frac{\sigma_E + \rho_S S \frac{\eta}{\eta + \mu_S} + \rho_R R \frac{\eta}{\eta + \mu_R}}{\eta S \frac{\mu_S}{\eta + \mu_S} + \eta R \frac{\mu_R}{\eta + \mu_R} + \delta_E}$$

$$E_S = \frac{\rho_S + \eta E_E^*}{\eta + \mu_S}$$

$$E_R = \frac{\rho_R + \eta E_E^*}{\eta + \mu_R},$$

showing that the intra- and extracellular concentrations depend on the net balance between sources and sinks of facilitation factors. Inhibitors of the production of facilitation factors will reduce the intra and extracellular inputs to E (σ and ρ). In contrast drugs targeting facilitation factor receptors will reduce the binding of intracellular factors, reducing μ by some factor.

Coupling facilitation factor dynamics with cancer coculture spheroid growth

The cellular level description of facilitation was next scaled to describe the populations of resistant and sensitive cells competing and facilitating in coculture spheroids over time. The resistant and sensitive cells are described as transitioning between proliferative (P), quiescent (Z) and senescent (X) states.

Resource competition between all cells is described by $\alpha(P, Z, X) = 1 - \sum_{i=1}^{n} \frac{P_i + Z_i + X_i}{K_i}$, where competitive ability of each cell type (i) is determined by the carrying capacity parameter K_i.

Proliferative cells enter the G1/S phase cell cycle checkpoint at a baseline rate (r), which is reduced by resource competition and increased by facilitation factor availability (E). This beneficial facilitation factor effect saturates at high concentrations when uptake and binding becomes rate limited (c). The proliferation rate of resistant and sensitive cells will be related to the binding of intracellularly available facilitation factors ($\mu_i E_i$). The G1/S phase entry of cells of type i, based on competition and the internal concentration of facilitation factors therefore follows:

$$G_i = r_i\left(1 + \frac{\mu_i E_i}{1 + c\mu_i E_i}\right)\alpha(P, Z, X).$$

After entering the cell cycle checkpoint, cells undertake the decision to divide or enter a quiescent state, based on the balance of key regulatory cell cycle promoters and inhibitors. In addition to a baseline quiescence rate (λ_i), cells are promoted to enter the quiescent state by the cell cycle inhibitor ribociclib (x), which inactivates the key regulators of the G1/S phase cell cycle checkpoint (CDK4/6), blocking cell cycle progression. We describe the effect of ribociclib in inhibiting cell cycle progression and driving cells into a quiescent state as increasing with drug concentration following:

$$q_i(x) = \frac{x}{k_i + x}.$$

No additional quiescence is induced in the absence of treatment, complete cell cycle arrest is achieved at very high levels of ribociclib and the half maximal cell cycle arrest is achieved at a dose k_i for cell type i. Differences in this parameter between resistant and sensitive cells describes innate resistance to the drug that emerged through selection. Following quiescence, we describe the transition of cells into a senescent state at rate φ_i before cell death occurs at rate δ_i.

Combining these models of competition, facilitation, cell cycle progression, arrest and cell death yields the following spheroid population model, describing the abundance of proliferative quiescent and senescent resistant and sensitive cells in coculture spheroids over time. The dynamics of the extracellular facilitation factor concentration in the spheroid population model is governed by the balance between net secretion by proliferative and quiescent cells (resistant= γ_R and sensitive= γ_S) and its decay (δ_E), giving:

$$\frac{dP_i}{dt} = \left(G_i\left(1 - q_i(x)\right) - G_i q_i(x) - \lambda_i \right) P_i$$

$$\frac{dZ_i}{dt} = \left(G_i q_i(x) + \lambda_i\right) P_i - \varphi_i Z_i$$

$$\frac{dX_i}{dt} = \varphi_i Z_i - \delta_i X_i$$

$$\frac{dE_E}{dt} = \left(\sum \gamma_i (P_i + Z_i)\right) - \delta_E E_E.$$

Equation (6)

Resistant and sensitive cell coculture spheroid growth and facilitation across drug doses

Resistant and sensitive cells were fluorescently labeled as previously described in methods (***Lentiviral labeling of sensitive and resistant cells***) and replicate populations (n=3) were plated either in monoculture or in 50:50 initial coculture. Cancer spheroids were grown in 3D culture for 21 days with imaging performed at 3-4 day intervals and the abundance of each cell type enumerated as described previously in methods (***Mono- and coculture spheroid experiments***). To explore the consequence of cell-cell interactions of drug response, the replicated mono- and coculture time course experiments were conducted under 8 ribociclib concentrations within the EC20-50 range (0,100,200,400,600,800,1000,2000nM). Spheroid analysis and cell counts performed as described previously in methods (***Mono- and coculture spheroid experiments***).

Measuring the strength of competitive and facilitative interactions between subclones and vital cellular rates

We measured the strength of competitive and facilitative interactions between subclones, the drug impacts on cell cycle arrest and the vital cellular rates of proliferation, quiescence and senescence, by fitting the spheroid population model to the experimental data described above. Given the initial spheroid size and composition and the ribociclib concentration, the spheroid population model projects the abundance of sensitive and resistant cells throughout the experiment based on a given combination of biological rates. A log-normal distribution measurement model was used to

evaluate the likelihood of each spheroid abundance observation and weakly informative Bayesian priors were used in all cases (Supp. methods). The biological rates of each process in the spheroid population model were inferred with uncertainty, using Bayesian Hamiltonian Monte Carlo (HMC) (61). Biological rates were identified that yield the most accurate model predictions of the observed spheroid growth trajectories and composition over time and across all drug doses. The HMC algorithm efficiently samples the posterior distribution, describing the likely biological rates given the model, using derivatives of the probability density function. As a result, the inference approach jointly and efficiently: i) identifies the most probable range of subclone interaction strengths (competition and facilitation), ii) predicts the cellular composition and estradiol concentration throughout the experiments and iii) provides a probabilistic measurement of the likelihood of the hypothesis encoded by the model given the available data.

Model predictions of final spheroid size when modulating the strength of facilitation

To explore the consequences of blocking facilitation, we analyzed the impact on resistant and sensitive cell abundances of reducing the rate of receptor binding with facilitation factors (e.g. estradiol). The most likely values of the receptor binding parameters of each cell type (μ_S and μ_R) were reduced by a factor ζ (between 0 and 80% reduction). Using the model and holding all other parameters constant, the predicted abundance of sensitive and resistant cells after 21 days of coculture was forecasted, assuming continuous facilitation blocking throughout this period.

Acknowledgements

The authors would like to acknowledge the professional support of the Analytical Pharmacology Core of City of Hope National Medical Center, led by Dr. Tim Synold. The authors also thank Dr. Adam Cohen, Dr. Benjamin Decato, Dr. Jeffrey Chang, Dr. Phillip Moos, and Patrick Cosgrove for their comments on the manuscript. RSS was supported by the CSBC/PS-ON Summer Undergraduate Research Program. This research and JIG, FRA, and AHB have been supported by an NIH NCI U54CA209978 and 1U01CA264620-01 grants from the National Cancer Institute.

Author contributions

RE carried out experiments, was involved in their analysis and wrote the manuscript. JIG and FRA carried out the mathematical modeling and facilitation analysis and wrote the manuscript. VKG generated cell lines, performed experiments, and developed system for growth measurements. AHB conceived the study, was involved in data analysis, and wrote the manuscript. RSS developed the preliminary mathematical models. AN, JC, and EFM carried out RNA sequencing analysis. All authors approved the final version of the manuscript.

Competing interests

The authors declare no competing interests.

766 ## Data availability

767 All data involving results and conclusions are provided as supplemental data with this manuscript.

768

769

770 ## References:

771 1. Rozeboom B, Dey N, De P. ER+ metastatic breast cancer: past, present, and a prescription for an
772 apoptosis-targeted future. American journal of cancer research. 2019;9(12):2821-31. PubMed PMID:
773 31911865; PMCID: 6943351.
774 2. Kantarjian HM, Wolff RA. The MD Anderson manual of medical oncology: McGraw Hill
775 Professional; 2011.
776 3. Ries L, Melbert D, Krapcho M, Stinchcomb D, Howlader N, Horner M, Mariotto A, Miller B, Feuer
777 E, Altekruse SJB, MD: National Cancer Institute. SEER cancer statistics review, 1975–20052008;2999.
778 4. Yu Q, Sicinska E, Geng Y, Ahnstrom M, Zagozdzon A, Kong Y, Gardner H, Kiyokawa H, Harris LN,
779 Stal O, Sicinski P. Requirement for CDK4 kinase function in breast cancer. Cancer cell. 2006;9(1):23-32.
780 doi: 10.1016/j.ccr.2005.12.012. PubMed PMID: 16413469.
781 5. Yu Q, Geng Y, Sicinski P. Specific protection against breast cancers by cyclin D1 ablation. Nature.
782 2001;411(6841):1017-21. doi: 10.1038/35082500. PubMed PMID: 11429595.
783 6. Landis MW, Pawlyk BS, Li T, Sicinski P, Hinds PW. Cyclin D1-dependent kinase activity in murine
784 development and mammary tumorigenesis. Cancer cell. 2006;9(1):13-22. doi: 10.1016/j.ccr.2005.12.019.
785 PubMed PMID: 16413468.
786 7. Company ELa. Endocrine Therapy With or Without Abemaciclib (LY2835219) Following Surgery in
787 Participants With Breast Cancer (monarchE) 2017 [updated September 18, 2020; cited 2020 October 13].
788 Available from: https://www.clinicaltrials.gov/ct2/show/NCT03155997.
789 8. Pharmaceuticals N. A Trial to Evaluate Efficacy and Safety of Ribociclib With Endocrine Therapy as
790 Adjuvant Treatment in Patients With HR+/HER2- Early Breast Cancer (NATALEE) 2018 [updated October
791 2, 2020; cited 2020 October 13]. Available from: https://clinicaltrials.gov/ct2/show/NCT03701334.
792 9. Bertagnolli M ME, DeMichele A, Gnant M. PALbociclib CoLlaborative Adjuvant Study (PALLAS)
793 2015 [updated March 9, 2020; cited 2020 October 2013]. Available from:
794 https://clinicaltrials.gov/ct2/show/NCT02513394.
795 10. PENELOPE-B TRIAL OF IBRANCE® (PALBOCICLIB) IN EARLY BREAST CANCER DID NOT MEET
796 PRIMARY ENDPOINT: Pfizer; 2020 [updated October 9, 2020; cited 2020 October 13]. Available from:
797 https://www.pfizer.com/news/press-release/press-release-detail/penelope-b-trial-ibrancer-palbociclib-
798 early-breast-cancer.
799 11. Johnston S, Puhalla S, Wheatley D, Ring A, Barry P, Holcombe C, Boileau JF, Provencher L, Robidoux
800 A, Rimawi M, McIntosh SA, Shalaby I, Stein RC, Thirlwell M, Dolling D, Morden J, Snowdon C, Perry S,
801 Cornman C, Batten LM, Jeffs LK, Dodson A, Martins V, Modi A, Osborne CK, Pogue-Geile KL, Cheang MCU,
802 Wolmark N, Julian TB, Fisher K, MacKenzie M, Wilcox M, Huang Bartlett C, Koehler M, Dowsett M, Bliss
803 JM, Jacobs SA. Randomized Phase II Study Evaluating Palbociclib in Addition to Letrozole as Neoadjuvant
804 Therapy in Estrogen Receptor-Positive Early Breast Cancer: PALLET Trial. J Clin Oncol. 2019;37(3):178-89.
805 Epub 2018/12/14. doi: 10.1200/jco.18.01624. PubMed PMID: 30523750.
806 12. Johnston SRD, Harbeck N, Hegg R, Toi M, Martin M, Shao ZM, Zhang QY, Martinez Rodriguez JL,
807 Campone M, Hamilton E, Sohn J, Guarneri V, Okada M, Boyle F, Neven P, Cortés J, Huober J, Wardley A,
808 Tolaney SM, Cicin I, Smith IC, Frenzel M, Headley D, Wei R, San Antonio B, Hulstijn M, Cox J, O'Shaughnessy
809 J, Rastogi P. Abemaciclib Combined With Endocrine Therapy for the Adjuvant Treatment of HR+, HER2-,

Node-Positive, High-Risk, Early Breast Cancer (monarchE). J Clin Oncol. 2020;38(34):3987-98. Epub 2020/09/22. doi: 10.1200/jco.20.02514. PubMed PMID: 32954927; PMCID: PMC7768339.

13. Griffiths JI, Chen J, Cosgrove PA, O'Dea A, Sharma P, Ma C, Trivedi M, Kalinsky K, Wisinski KB, O'Regan R, Makhoul I, Spring LM, Bardia A, Adler FR, Cohen AL, Chang JT, Khan QJ, Bild AH. Serial single-cell genomics reveals convergent subclonal evolution of resistance as early-stage breast cancer patients progress on endocrine plus CDK4/6 therapy. Nat Cancer. 2021;2(6):658-71. Epub 2021/10/30. doi: 10.1038/s43018-021-00215-7. PubMed PMID: 34712959; PMCID: PMC8547038.

14. Finn RS, Martin M, Rugo HS, Jones S, Im SA, Gelmon K, Harbeck N, Lipatov ON, Walshe JM, Moulder S, Gauthier E, Lu DR, Randolph S, Dieras V, Slamon DJ. Palbociclib and Letrozole in Advanced Breast Cancer. N Engl J Med. 2016;375(20):1925-36. Epub 2016/12/14. doi: 10.1056/NEJMoa1607303. PubMed PMID: 27959613.

15. Fan W, Chang J, Fu P. Endocrine therapy resistance in breast cancer: current status, possible mechanisms and overcoming strategies. Future Med Chem. 2015;7(12):1511-9. Epub 2015/08/27. doi: 10.4155/fmc.15.93. PubMed PMID: 26306654; PMCID: PMC5558537.

16. McGranahan N, Swanton C. Clonal Heterogeneity and Tumor Evolution: Past, Present, and the Future. Cell. 2017;168(4):613-28. doi: 10.1016/j.cell.2017.01.018. PubMed PMID: 28187284.

17. Brady SW, McQuerry JA, Qiao Y, Piccolo SR, Shrestha G, Jenkins DF, Layer RM, Pedersen BS, Miller RH, Esch A, Selitsky SR, Parker JS, Anderson LA, Dalley BK, Factor RE, Reddy CB, Boltax JP, Li DY, Moos PJ, Gray JW, Heiser LM, Buys SS, Cohen AL, Johnson WE, Quinlan AR, Marth G, Werner TL, Bild AH. Combating subclonal evolution of resistant cancer phenotypes. Nature communications. 2017;8(1):1231. doi: 10.1038/s41467-017-01174-3. PubMed PMID: 29093439; PMCID: 5666005.

18. Delou JMA, Souza ASO, Souza LCM, Borges HL. Highlights in Resistance Mechanism Pathways for Combination Therapy. Cells. 2019;8(9). doi: 10.3390/cells8091013. PubMed PMID: 31480389; PMCID: 6770082.

19. Fedele C, Tothill RW, McArthur GA. Navigating the challenge of tumor heterogeneity in cancer therapy. Cancer discovery. 2014;4(2):146-8. doi: 10.1158/2159-8290.CD-13-1042. PubMed PMID: 24501303.

20. Swanton C. Intratumor heterogeneity: evolution through space and time. Cancer research. 2012;72(19):4875-82. doi: 10.1158/0008-5472.CAN-12-2217. PubMed PMID: 23002210; PMCID: 3712191.

21. Franco OE, Tyson DR, Konvinse KC, Udyavar AR, Estrada L, Quaranta V, Crawford SE, Hayward SW. Altered TGF-alpha/beta signaling drives cooperation between breast cancer cell populations. FASEB journal : official publication of the Federation of American Societies for Experimental Biology. 2016;30(10):3441-52. doi: 10.1096/fj.201500187RR. PubMed PMID: 27383183; PMCID: 5024699.

22. Gatenby RA, Brown JS. The Evolution and Ecology of Resistance in Cancer Therapy. Cold Spring Harbor perspectives in medicine. 2020;10(11). doi: 10.1101/cshperspect.a040972. PubMed PMID: 33139405; PMCID: 7605238.

23. Heppner GH. Cancer cell societies and tumor progression. Stem cells. 1993;11(3):199-203. doi: 10.1002/stem.5530110306. PubMed PMID: 8318906.

24. Pienta KJ, McGregor N, Axelrod R, Axelrod DE. Ecological therapy for cancer: defining tumors using an ecosystem paradigm suggests new opportunities for novel cancer treatments. Translational oncology. 2008;1(4):158-64. doi: 10.1593/tlo.08178. PubMed PMID: 19043526; PMCID: 2582164.

25. Crespi B, Summers K. Evolutionary biology of cancer. Trends in ecology & evolution. 2005;20(10):545-52. doi: 10.1016/j.tree.2005.07.007. PubMed PMID: 16701433.

26. Sieber OM, Tomlinson SR, Tomlinson IP. Tissue, cell and stage specificity of (epi)mutations in cancers. Nature reviews Cancer. 2005;5(8):649-55. doi: 10.1038/nrc1674. PubMed PMID: 16056260.

27. Gatenby RA, Vincent TL. Application of quantitative models from population biology and evolutionary game theory to tumor therapeutic strategies. Molecular cancer therapeutics. 2003;2(9):919-27. PubMed PMID: 14555711.
28. Oates K, Wilson M. Nominal kinship cues facilitate altruism. Proceedings Biological sciences. 2002;269(1487):105-9. doi: 10.1098/rspb.2001.1875. PubMed PMID: 11798424; PMCID: 1690876.
29. Wilson DS, Pollock GB, Dugatkin LA. Can Altruism Evolve in Purely Viscous Populations. Evol Ecol. 1992;6(4):331-41. doi: Doi 10.1007/Bf02270969. PubMed PMID: WOS:A1992JD08100005.
30. Bruno JF, Stachowicz JJ, Bertness MD. Inclusion of facilitation into ecological theory. Trends in ecology & evolution. 2003;18(3):119-25. doi: Pii S0169-5347(02)00045-9
Doi 10.1016/S0169-5347(02)00045-9. PubMed PMID: WOS:000181729900007.
31. Caldwell MM, Dawson TE, Richards JH. Hydraulic lift: Consequences of water efflux from the roots of plants. Oecologia. 1998;113(2):151-61. doi: DOI 10.1007/s004420050363. PubMed PMID: WOS:000071658500001.
32. Grolmusz VK, Chen J, Emond R, Cosgrove PA, Pflieger L, Nath A, Moos PJ, Bild AH. Exploiting collateral sensitivity controls growth of mixed culture of sensitive and resistant cells and decreases selection for resistant cells in a cell line model. Cancer cell international. 2020;20:253. doi: 10.1186/s12935-020-01337-1. PubMed PMID: 32565737; PMCID: 7301982.
33. Bronzert DA, Greene GL, Lippman ME. Selection and characterization of a breast cancer cell line resistant to the antiestrogen LY 117018. Endocrinology. 1985;117(4):1409-17. doi: 10.1210/endo-117-4-1409. PubMed PMID: 4029083.
34. Mullick A, Chambon P. Characterization of the estrogen receptor in two antiestrogen-resistant cell lines, LY2 and T47D. Cancer research. 1990;50(2):333-8. PubMed PMID: 2295073.
35. Adler FR. Modeling the dynamics of life: calculus and probability for life scientists: Nelson Education; 2012.
36. Friesenhengst A, Pribitzer-Winner T, Miedl H, Prostling K, Schreiber M. Elevated Aromatase (CYP19A1) Expression Is Associated with a Poor Survival of Patients with Estrogen Receptor Positive Breast Cancer. Hormones & cancer. 2018;9(2):128-38. doi: 10.1007/s12672-017-0317-2. PubMed PMID: 29363090; PMCID: 5862917.
37. Mukhopadhyay KD, Liu Z, Bandyopadhyay A, Kirma NB, Tekmal RR, Wang S, Sun LZ. Aromatase expression increases the survival and malignancy of estrogen receptor positive breast cancer cells. PloS one. 2015;10(4):e0121136. doi: 10.1371/journal.pone.0121136. PubMed PMID: 25837259; PMCID: 4383596.
38. Neven P, Sonke GS, Jerusalem G. Ribociclib plus fulvestrant in the treatment of breast cancer. Expert review of anticancer therapy. 2021;21(1):93-106. doi: 10.1080/14737140.2021.1840360. PubMed PMID: 33085548.
39. Im SA, Lu YS, Tripathy D. Ribociclib and Endocrine Therapy in Breast Cancer. Reply. N Engl J Med. 2019;381(16):1592-3. doi: 10.1056/NEJMc1911188. PubMed PMID: 31618550.
40. Tripathy D, Im SA, Colleoni M, Franke F, Bardia A, Harbeck N, Hurvitz SA, Chow L, Sohn J, Lee KS, Campos-Gomez S, Villanueva Vazquez R, Jung KH, Babu KG, Wheatley-Price P, De Laurentiis M, Im YH, Kuemmel S, El-Saghir N, Liu MC, Carlson G, Hughes G, Diaz-Padilla I, Germa C, Hirawat S, Lu YS. Ribociclib plus endocrine therapy for premenopausal women with hormone-receptor-positive, advanced breast cancer (MONALEESA-7): a randomised phase 3 trial. The Lancet Oncology. 2018;19(7):904-15. doi: 10.1016/S1470-2045(18)30292-4. PubMed PMID: 29804902.
41. Kalas W, Yu JL, Milsom C, Rosenfeld J, Benezra R, Bornstein P, Rak J. Oncogenes and Angiogenesis: down-regulation of thrombospondin-1 in normal fibroblasts exposed to factors from cancer cells harboring mutant ras. Cancer research. 2005;65(19):8878-86. doi: 10.1158/0008-5472.CAN-05-1479. PubMed PMID: 16204059.

903 42. Hanahan D, Folkman J. Patterns and Emerging Mechanisms of the Angiogenic Switch during
904 Tumorigenesis. Cell. 1996;86(3):353-64. doi: https://doi.org/10.1016/S0092-8674(00)80108-7.
905 43. Archetti M, Pienta KJ. Cooperation among cancer cells: applying game theory to cancer. Nature
906 reviews Cancer. 2019;19(2):110-7. Epub 2018/11/25. doi: 10.1038/s41568-018-0083-7. PubMed PMID:
907 30470829.
908 44. Cleary AS, Leonard TL, Gestl SA, Gunther EJ. Tumour cell heterogeneity maintained by cooperating
909 subclones in Wnt-driven mammary cancers. Nature. 2014;508(7494):113-7. doi: 10.1038/nature13187.
910 PubMed PMID: 24695311; PMCID: 4050741.
911 45. Naffar-Abu Amara S, Kuiken HJ, Selfors LM, Butler T, Leung ML, Leung CT, Kuhn EP, Kolarova T,
912 Hage C, Ganesh K, Panayiotou R, Foster R, Rueda BR, Aktipis A, Spellman P, Ince TA, Xiu J, Oberley M,
913 Gatalica Z, Navin N, Mills GB, Bronson RT, Brugge JS. Transient commensal clonal interactions can drive
914 tumor metastasis. Nature communications. 2020;11(1):5799. doi: 10.1038/s41467-020-19584-1. PubMed
915 PMID: 33199705; PMCID: 7669858.
916 46. Archetti M, Ferraro DA, Christofori G. Heterogeneity for IGF-II production maintained by public
917 goods dynamics in neuroendocrine pancreatic cancer. Proceedings of the National Academy of Sciences
918 of the United States of America. 2015;112(6):1833-8. doi: 10.1073/pnas.1414653112. PubMed PMID:
919 25624490; PMCID: 4330744.
920 47. Kefi S, van Baalen M, Rietkerk M, Loreau M. Evolution of local facilitation in arid ecosystems. The
921 American naturalist. 2008;172(1):E1-17. doi: 10.1086/588066. PubMed PMID: 18554137.
922 48. Bertness MD, Callaway R. Positive interactions in communities. Trends in ecology & evolution.
923 1994;9(5):191-3. doi: 10.1016/0169-5347(94)90088-4. PubMed PMID: 21236818.
924 49. Simigdala N, Gao Q, Pancholi S, Roberg-Larsen H, Zvelebil M, Ribas R, Folkerd E, Thompson A,
925 Bhamra A, Dowsett M, Martin L-A. Cholesterol biosynthesis pathway as a novel mechanism of resistance
926 to estrogen deprivation in estrogen receptor-positive breast cancer. Breast Cancer Research.
927 2016;18(1):58. doi: 10.1186/s13058-016-0713-5.
928 50. Harada N. Aberrant expression of aromatase in breast cancer tissues. J Steroid Biochem Mol Biol.
929 1997;61(3-6):175-84. Epub 1997/04/01. PubMed PMID: 9365188.
930 51. Forbes NS, Meadows AL, Clark DS, Blanch HW. Estradiol stimulates the biosynthetic pathways of
931 breast cancer cells: detection by metabolic flux analysis. Metabolic engineering. 2006;8(6):639-52. doi:
932 10.1016/j.ymben.2006.06.005. PubMed PMID: 16904360.
933 52. Platet N, Cathiard AM, Gleizes M, Garcia M. Estrogens and their receptors in breast cancer
934 progression: a dual role in cancer proliferation and invasion. Critical reviews in oncology/hematology.
935 2004;51(1):55-67. doi: 10.1016/j.critrevonc.2004.02.001. PubMed PMID: 15207254.
936 53. AlFakeeh A, Brezden-Masley C. Overcoming endocrine resistance in hormone receptor-positive
937 breast cancer. Curr Oncol. 2018;25(Suppl 1):S18-s27. Epub 2018/06/19. doi: 10.3747/co.25.3752.
938 PubMed PMID: 29910644; PMCID: PMC6001756.
939 54. Gonzalez-Angulo AM, Morales-Vasquez F, Hortobagyi GN. Overview of resistance to systemic
940 therapy in patients with breast cancer. Adv Exp Med Biol. 2007;608:1-22. Epub 2007/11/13. doi:
941 10.1007/978-0-387-74039-3_1. PubMed PMID: 17993229.
942 55. Pepper JW. Drugs that target pathogen public goods are robust against evolved drug resistance.
943 Evolutionary applications. 2012;5(7):757-61. doi: 10.1111/j.1752-4571.2012.00254.x. PubMed PMID:
944 23144661; PMCID: 3492900.
945 56. Stuart T, Butler A, Hoffman P, Hafemeister C, Papalexi E, Mauck WM, 3rd, Hao Y, Stoeckius M,
946 Smibert P, Satija R. Comprehensive Integration of Single-Cell Data. Cell. 2019;177(7):1888-902 e21. doi:
947 10.1016/j.cell.2019.05.031. PubMed PMID: 31178118; PMCID: 6687398.
948 57. Wolock SL, Lopez R, Klein AM. Scrublet: Computational Identification of Cell Doublets in Single-
949 Cell Transcriptomic Data. Cell systems. 2019;8(4):281-91 e9. doi: 10.1016/j.cels.2018.11.005. PubMed
950 PMID: 30954476; PMCID: 6625319.

951 58. Finak G, McDavid A, Yajima M, Deng J, Gersuk V, Shalek AK, Slichter CK, Miller HW, McElrath MJ,
952 Prlic M, Linsley PS, Gottardo R. MAST: a flexible statistical framework for assessing transcriptional changes
953 and characterizing heterogeneity in single-cell RNA sequencing data. Genome biology. 2015;16:278. doi:
954 10.1186/s13059-015-0844-5. PubMed PMID: 26653891; PMCID: 4676162.
955 59. Liberzon A, Birger C, Thorvaldsdottir H, Ghandi M, Mesirov JP, Tamayo P. The Molecular
956 Signatures Database (MSigDB) hallmark gene set collection. Cell systems. 2015;1(6):417-25. doi:
957 10.1016/j.cels.2015.12.004. PubMed PMID: 26771021; PMCID: 4707969.
958 60. Hanzelmann S, Castelo R, Guinney J. GSVA: gene set variation analysis for microarray and RNA-
959 seq data. BMC bioinformatics. 2013;14:7. doi: 10.1186/1471-2105-14-7. PubMed PMID: 23323831;
960 PMCID: 3618321.
961 61. Carpenter B, Gelman A, Hoffman MD, Lee D, Goodrich B, Betancourt M, Brubaker MA, Guo J, Li P,
962 Riddell A. Stan: a probabilistic programming language. Grantee Submission. 2017;76(1):1-32.
963

964

965 # Figure Legends

966 ***Figure 1.*** **Sensitive and resistant cell growth, treatment effects, and ribociclib induced facilitation.**
967 **a,** CAMA-1 spheroids of 100% monoculture sensitive (venus, green) or resistant cells (cerulean, blue)
968 cultured in untreated control, 200 nM ribociclib, and 400nM ribociclib treated medium for 18 days.
969 Images taken at Day 18. **b,** Growth curves of CAMA-1 untreated and ribociclib treated (400 nM) sensitive
970 and resistant cell populations. **c,** CAMA-1 spheroids of different cell compositions (100% sensitive -
971 green, 50% sensitive- 50% resistant, 100% resistant - blue) cultured in untreated, 200 nM ribociclib, and
972 400 nM ribociclib treated medium for 18 days. Images taken at Day 18 **d,** Box plot of CAMA-1 log fold
973 change of untreated and ribociclib treated (400 nM) sensitive or resistant cells from day 0 to day 14 in
974 monoculture and coculture (n=3). In monoculture, sensitive cells have a significantly higher reduction in
975 growth than resistant cells ($p<0.0001$). Sensitive cells have a significantly lower growth reduction in
976 coculture than in monoculture ($p < 0.0001$). Resistant cells show no significant effect ($p=0.2$) and a
977 significantly smaller change in growth due to treatment in coculture ($p=0.005$). **e,** Box plots of competitive
978 effect of sensitive (S) cells on resistant (R) cells and vice versa for CAMA-1 cells ($p=0.0023$ with a t test,
979 n=3). **f,** Facilitation measured as log observed growth relative to expected growth averaged over all
980 replicates for CAMA-1 cells ($p < 0.001$ for interaction of cell type with day using a linear model of the
981 log of observed over expected cell number as a function of time).

982 ***Figure 2.*** **Underlying biological processes driving facilitation in response to ribociclib treatment.**
983 **a**, Growth of CAMA-1 spheroids under drug pressure with supplemented conditioned media from
984 spheroids of different compositions. Sensitive and resistant cells were plated by the indicated composition
985 of sensitive and resistant cells in a 3D spheroid format and underwent exposure to untreated or 400nM
986 treated medium to produce conditioned media. 100% sensitive spheroids under drug pressure were then
987 supplemented with different concentrations of conditioned media. Normalized cell counts of sensitive
988 cells supplemented with untreated or treated conditioned media generated from different spheroid
989 compositions. **b,** Liquid chromatography-tandem mass spectrometry (LC-MS/MS) assay for estradiol
990 detection performed on CAMA-1 untreated or ribociclib 200nM treated samples of the following
991 compositions at Day 21: 100% sensitive, 50% sensitive – 50% resistant, 100% resistant samples. **c,**
992 Estradiol concentration by resistant and sensitive cell abundance; Estradiol production rates of CAMA-1
993 ribociclib sensitive and resistant cells and sensitive cell uptake of estradiol (relative to resistant cells) **d,**
994 diagram depicting CAMA-1 resistant and sensitive cell contributions of estradiol metabolism enzymes

995 HSD17β1 and HSD17β8. **e,** Western blot analysis of HSD17β1, HSD17β8, and β-actin (control) in
996 monoculture, untreated sensitive and resistant CAMA-1 cells.

997 ***Figure 3.*** **Modifying endocrine signaling pathways affects spheroid growth and facilitation. a,** CAMA-
998 1 spheroids of different cell compositions (100% sensitive - green, 50% sensitive- 50% resistant, 100%
999 resistant - blue) cultured in untreated, 400nM ribociclib, 0.1nM estradiol, or combination 400nM ribociclib
1000 with 0.1nM estradiol treated medium for 18 days; images taken on day 18. **b,** CAMA-1 spheroids of
1001 different cell compositions (100% sensitive - green, 50% sensitive- 50% resistant, 100% resistant - blue)
1002 cultured in untreated, 400nM ribociclib, 1nM or 3nM fulvestrant, or combination 400nM ribociclib with
1003 1nM or 3nM fulvestrant treated medium for 18 days; images taken on day 18. **c,** Sensitive cells with single
1004 treatment (n=3). When treated with ribociclib or fulvestrant, sensitive cells in coculture with resistant cells
1005 are significantly facilitated ($p<0.0001$) each with higher facilitation at higher doses ($p<0.0001$). Estradiol
1006 creates weak but significant negative facilitation ($p<0.05$). **d,** Sensitive cells with combination treatment
1007 (n=3). Compared with single treatment with ribociclib, combination treatment with estradiol significantly
1008 reduces facilitation ($p<0.0001$) although completely to 0 ($p=0.016$). The strength of facilitation is
1009 unchanged at the lower 1nM dose of fulvestrant and increased at the higher 3nM dose ($p=0.004$).

1010 ***Figure 4.*** **RNA sequencing reveals transcriptomic differences between mono- and cocultured sensitive**
1011 **and resistant cells. a,** UMAP of scRNA-seq profiles from 6292 resistant (coculture), 7557 resistant
1012 (monoculture), 2059 sensitive (coculture) and 3329 sensitive (monoculture) CAMA-1 cells. **b,** Cell
1013 phenotypic heterogeneity visualized using UMAP and colored according to cell phase estimated using the
1014 scRNA-seq profiles of CAMA-1 cells. Stacked bar plots on the right show proportion of cells within each
1015 phase of the cell cycle. **c,** Ridge density plots showing density of ssGSEA enrichment scores for cell cycle
1016 pathways across different cell lines. White vertical line indicates median of the distribution, with FDR
1017 adjusted p-value from Wilcoxon rank-sum test between sensitive monoculture vs. sensitive coculture
1018 indicated to the right. **d,** Ridge density plots showing density of ssGSEA enrichment scores for estrogen
1019 signaling response pathways across different cell lines. White vertical line indicates median of the
1020 distribution, with FDR adjusted p-value from Wilcoxon rank-sum test between sensitive monoculture vs.
1021 sensitive coculture indicated to the right. **e,** Dot plots showing gene expression levels measured in ribociclib
1022 resistant and sensitive cells using bulk RNA-seq. Each colored dot indicates one independent biological
1023 replicate, with the grey dot and bars indicating mean and standard deviations. The p-value indicate
1024 significance of difference in means from Welch's t-test.

1025 ***Figure 5.*** **Measuring the strength and role of facilitation during treatment**. **a,** Structure of mechanistic
1026 stage–structured differential equation model of facilitation fitted to data. This describes the abundance of
1027 resistant (red) and sensitive (green) cells which compete (circle headed arrows) and also facilitate one
1028 another through the production of facilitation factor (E; estradiol; blue) used by both cell types to promote
1029 cell division. Resistant and sensitive cells transition through proliferative (P), quiescent (Z) and then
1030 senescent (X) stages. Proliferative cells enter the G1/S cell cycle checkpoint at a rate that depends on
1031 competitor abundance and facilitation factor concentration. Upon entry to the G1/S cell cycle checkpoint,
1032 cells either divide or enter the quiescent state. Cell cycle inhibitor therapy prevents accumulation of cell
1033 cycle promoting proteins, increasing the fraction of cells entering the quiescent stage, rather than dividing.
1034 **b,** Predicted spheroid growth from initial abundance for sensitive and resistant cells (rows), alone or in co-
1035 culture (columns) and across a broad range of ribociclib doses (color). Observed cell counts over time
1036 (points) are accurately predicted across all doses and cell type compositions (lines) by the facilitation model
1037 and uncertainty in model fits are captured by the 95% high credibility intervals (shaded regions). **c,**
1038 Quantification of the resistant and sensitive cells' abilities to facilitate neighboring cell growth, compete
1039 for resources, divide or quiesce in the absence of therapy and to respond to the direct impacts of treatment

(drug sensitivity). Performance of resistant cells, relative to sensitive cells, is shown for each process (y axis), with the violin plots showing the range of relative performance values yielding spheroid trajectories consistent with the observed data (shaded region). Equal performance of the two cell types is signified by the vertical dashed line. **d,** Prediction of impacts of blocking facilitation on sensitive and resistant cell growth in co-culture, across drug dose. Datapoints show the observed final size of replicate spheroids across doses without facilitation blocking (100% facilitation). The thick black bordered lines show the facilitation model predictions of final size. Thinner lines show the predicted reduction in final abundance of resistant and sensitive cells achievable by reducing facilitation (brighter lines indicate greater facilitation levels). **e,** The role of facilitation on spheroid growth, relative to competition, across drug doses. Each point on the surface indicates a specific time and dose. The coloration shows how important facilitation is at that moment (brighter coloration indicates that facilitation is more important). The bright band shows the window of facilitation when abundance of both cell types is increasing but the carrying capacity (maximal density of the spheroid) is not reached.

a

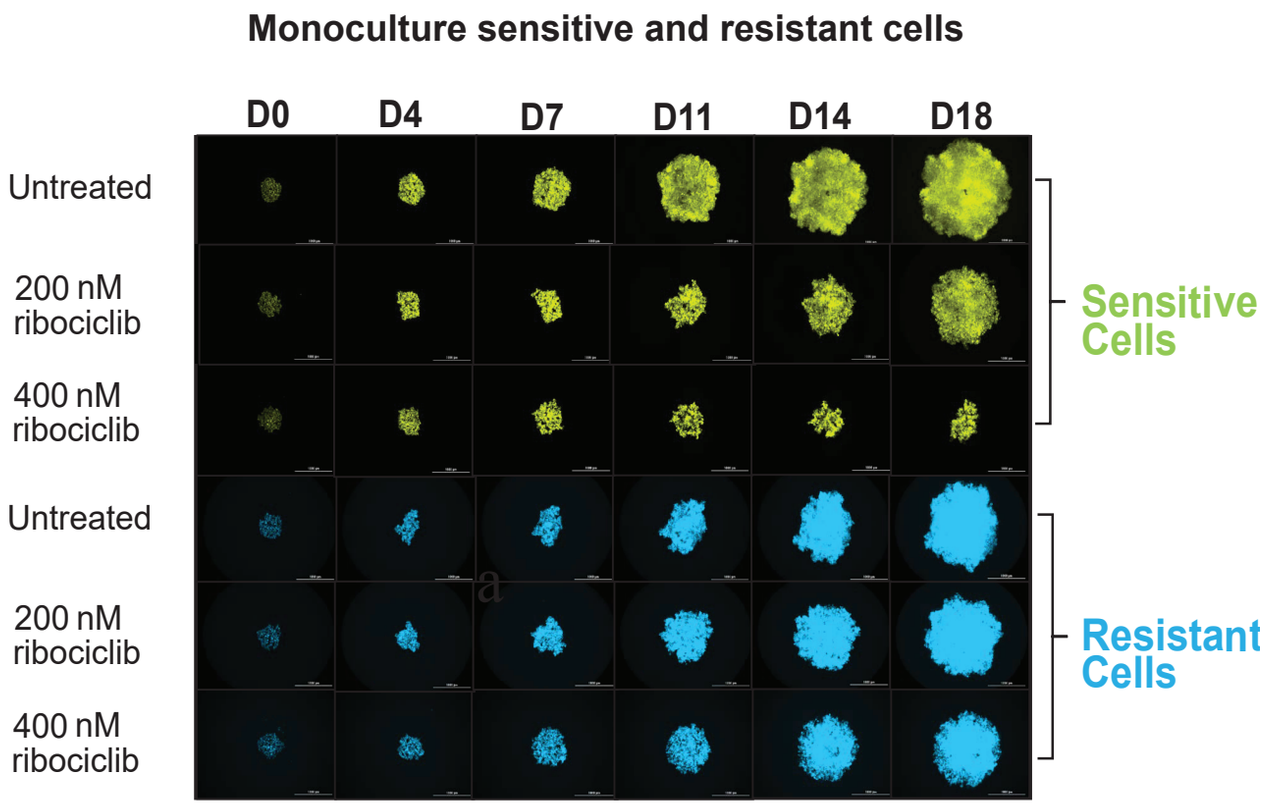
Monoculture sensitive and resistant cells
D0
D4
D7
D11
D14
D18
Untreated
200 nM ribociclib
400 nM ribociclib
Untreated
200 nM ribociclib
400 nM ribociclib
Sensitive Cells
Resistant Cells

b

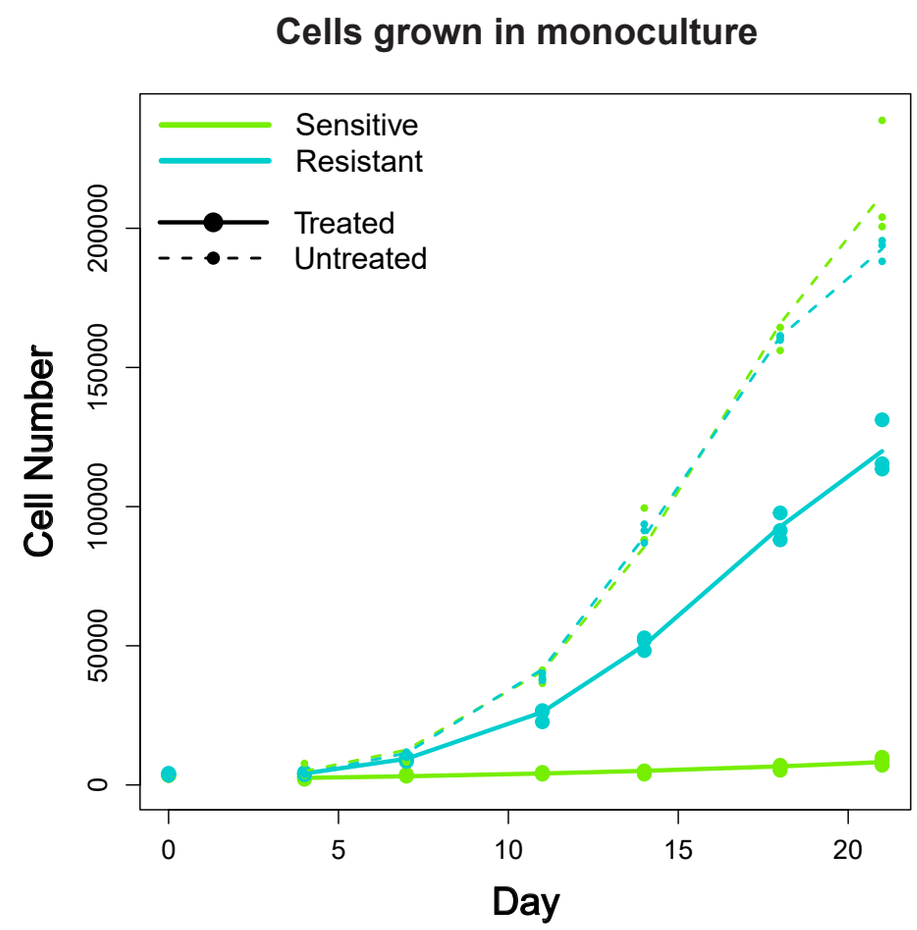
Cells grown in monoculture
Sensitive
Resistant
Treated
Untreated
Cell Number
0
50000
100000
150000
200000
0
5
10
15
20
Day

c

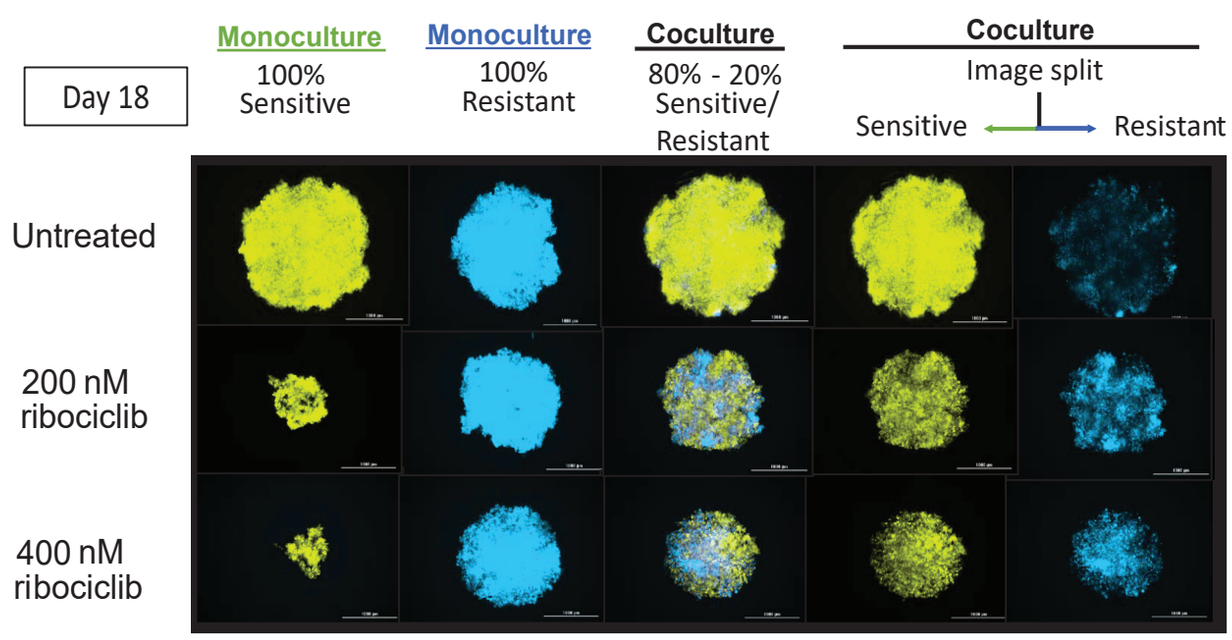
Day 18
Monoculture
100% Sensitive
Monoculture
100% Resistant
Coculture
80% - 20% Sensitive/ Resistant
Coculture
Image split
Sensitive
Resistant
Untreated
200 nM ribociclib
400 nM ribociclib

d

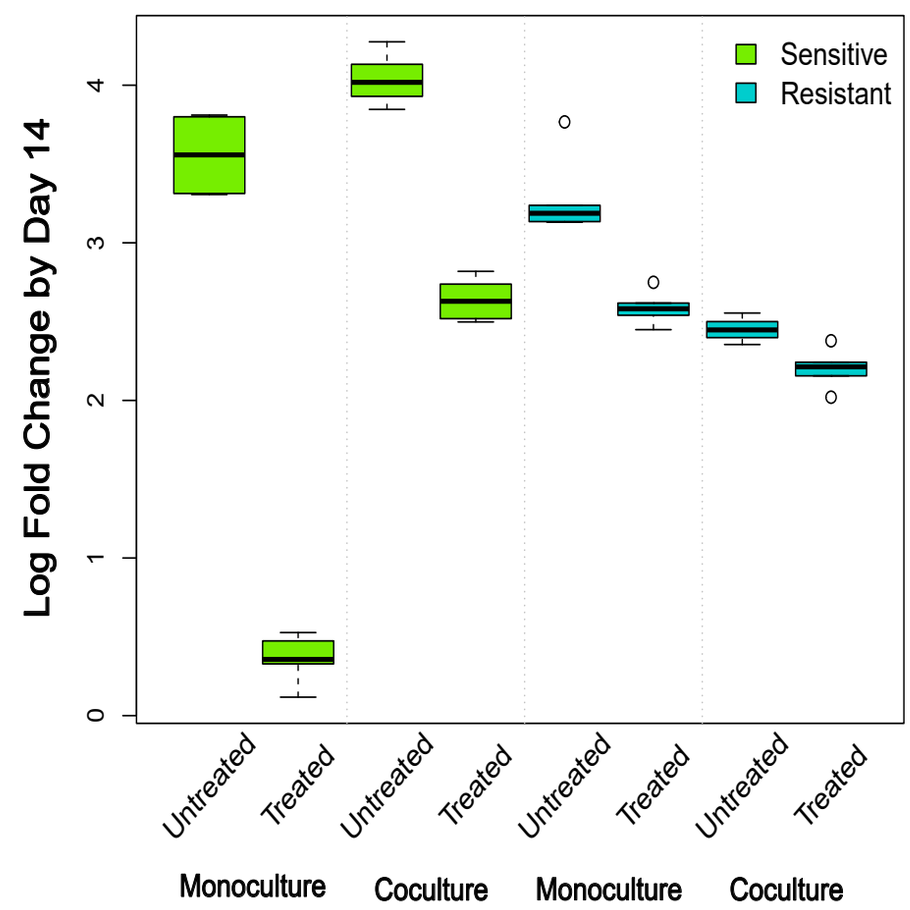
Sensitive
Resistant
Log Fold Change by Day 14
0
1
2
3
4
Untreated
Treated
Untreated
Treated
Untreated
Treated
Untreated
Treated
Monoculture
Coculture
Monoculture
Coculture

e

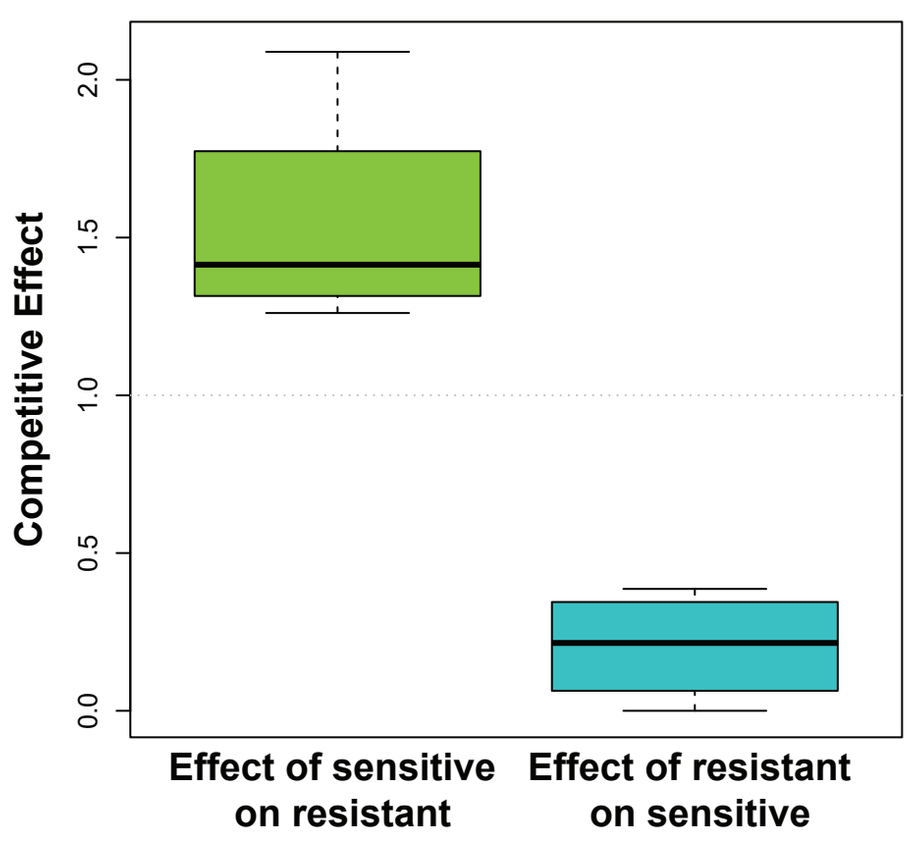
Competitive Effect
0.0
0.5
1.0
1.5
2.0
Effect of sensitive on resistant
Effect of resistant on sensitive

f

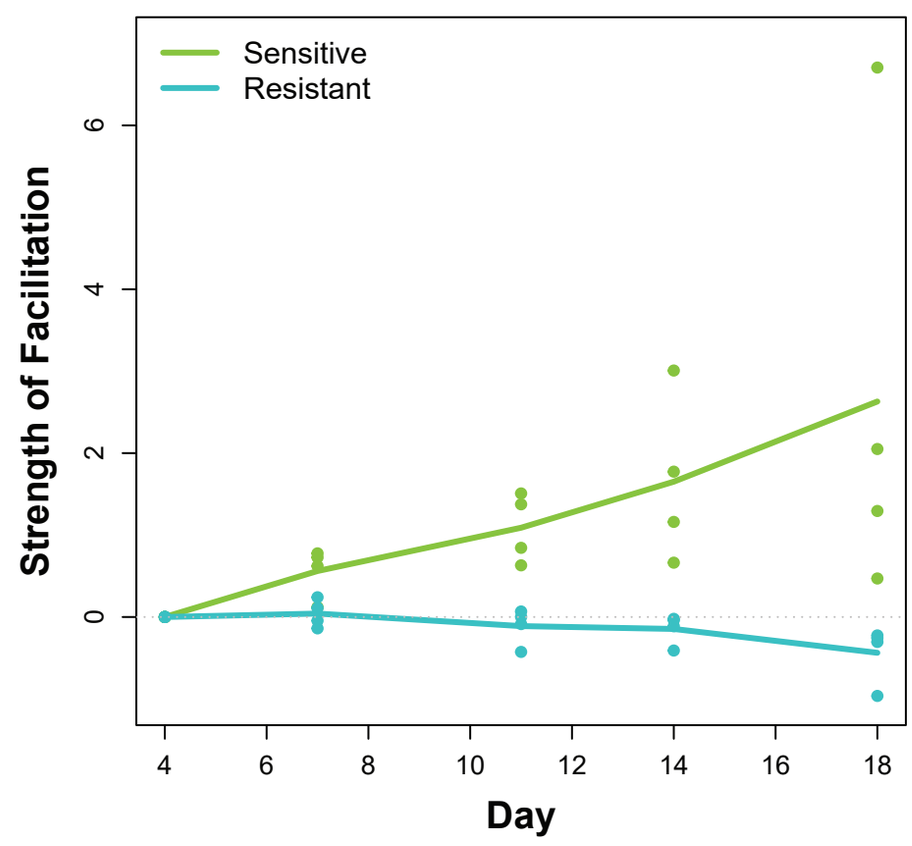
Sensitive
Resistant
Strength of Facilitation
0
2
4
6
4
6
8
10
12
14
16
18
Day

a

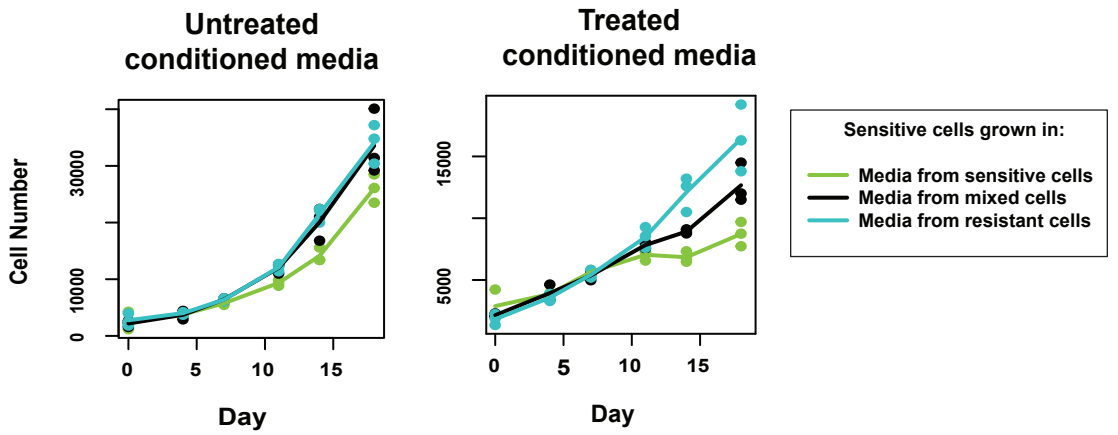
Untreated conditioned media
Treated conditioned media
Cell Number
0
10000
30000
5000
15000
0
5
10
15
Day
Sensitive cells grown in:
Media from sensitive cells
Media from mixed cells
Media from resistant cells

b

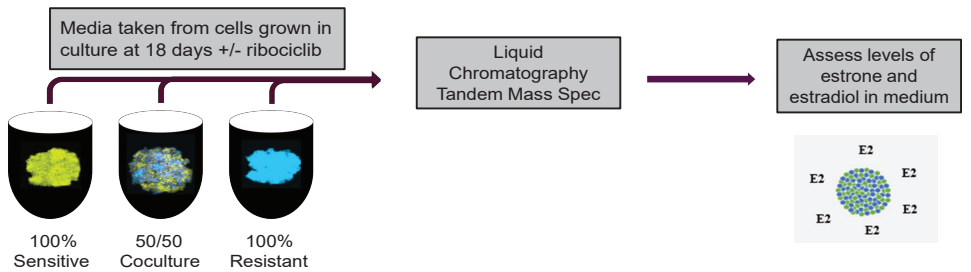
Media taken from cells grown in culture at 18 days +/- ribociclib
Liquid Chromatography Tandem Mass Spec
Assess levels of estrone and estradiol in medium
E2
100% Sensitive
50/50 Coculture
100% Resistant

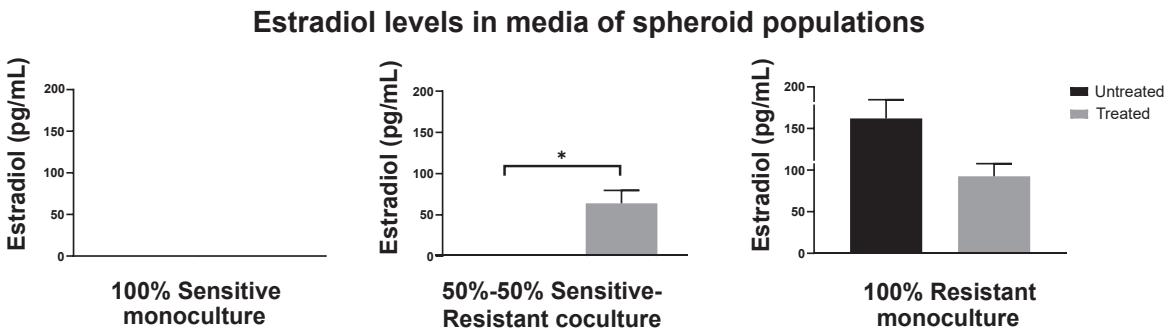
Estradiol levels in media of spheroid populations
Estradiol (pg/mL)
0
50
100
150
200
*
Untreated
Treated
100% Sensitive monoculture
50%-50% Sensitive-Resistant coculture
100% Resistant monoculture

c

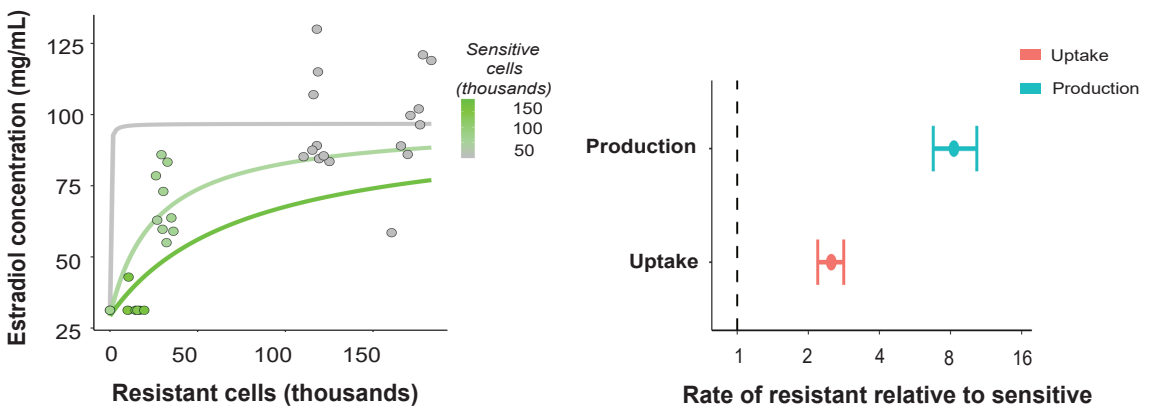
Estradiol concentration (mg/mL)
25
50
75
100
125
0
50
100
150
Resistant cells (thousands)
Sensitive cells (thousands)
150
100
50
Uptake
Production
1
2
4
8
16
Rate of resistant relative to sensitive

d

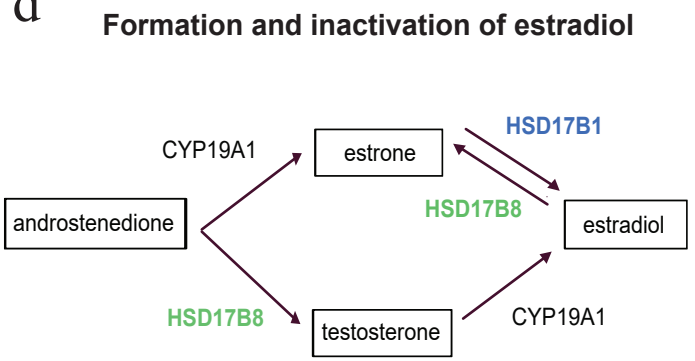
Formation and inactivation of estradiol
androstenedione
CYP19A1
estrone
HSD17B1
HSD17B8
estradiol
HSD17B8
testosterone
CYP19A1

e

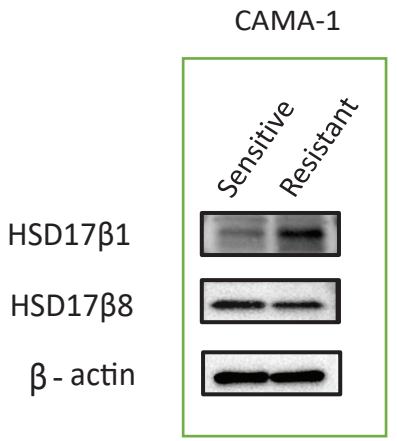
CAMA-1
Sensitive
Resistant
HSD17β1
HSD17β8
β - actin

a

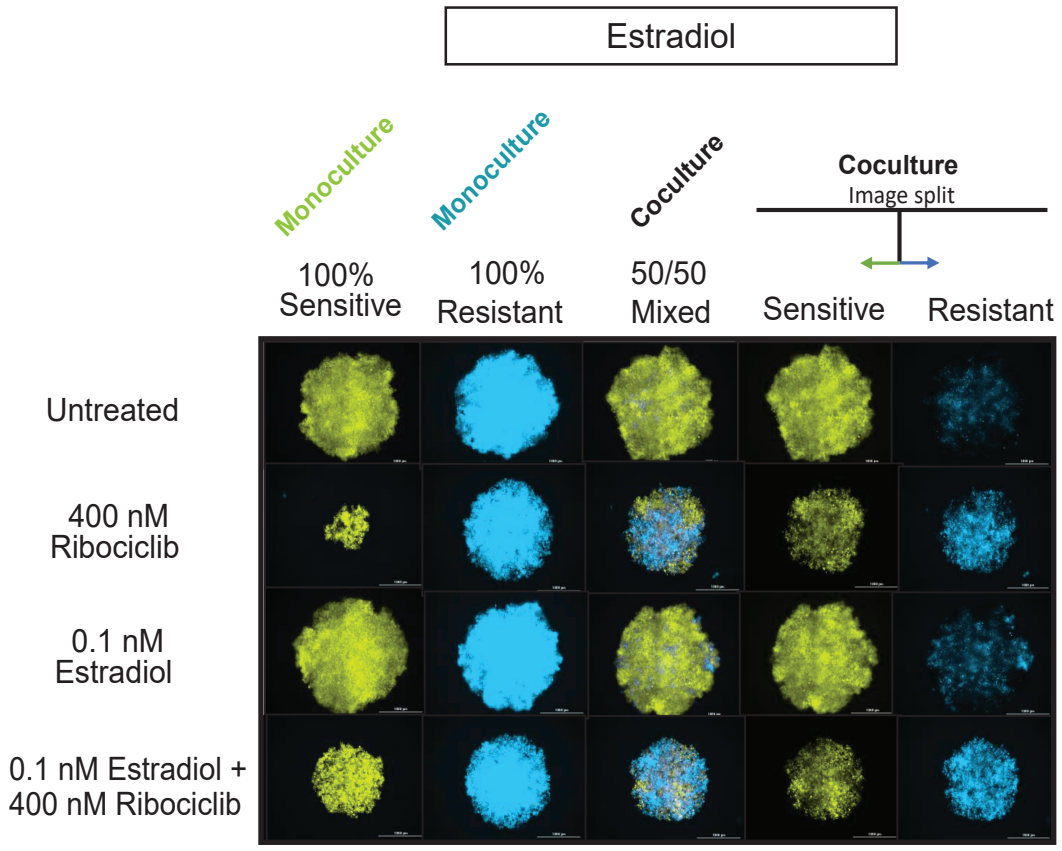
Estradiol
Monoculture
Monoculture
Coculture
Coculture
Image split
100% Sensitive
100% Resistant
50/50 Mixed
Sensitive
Resistant
Untreated
400 nM Ribociclib
0.1 nM Estradiol
0.1 nM Estradiol + 400 nM Ribociclib

c

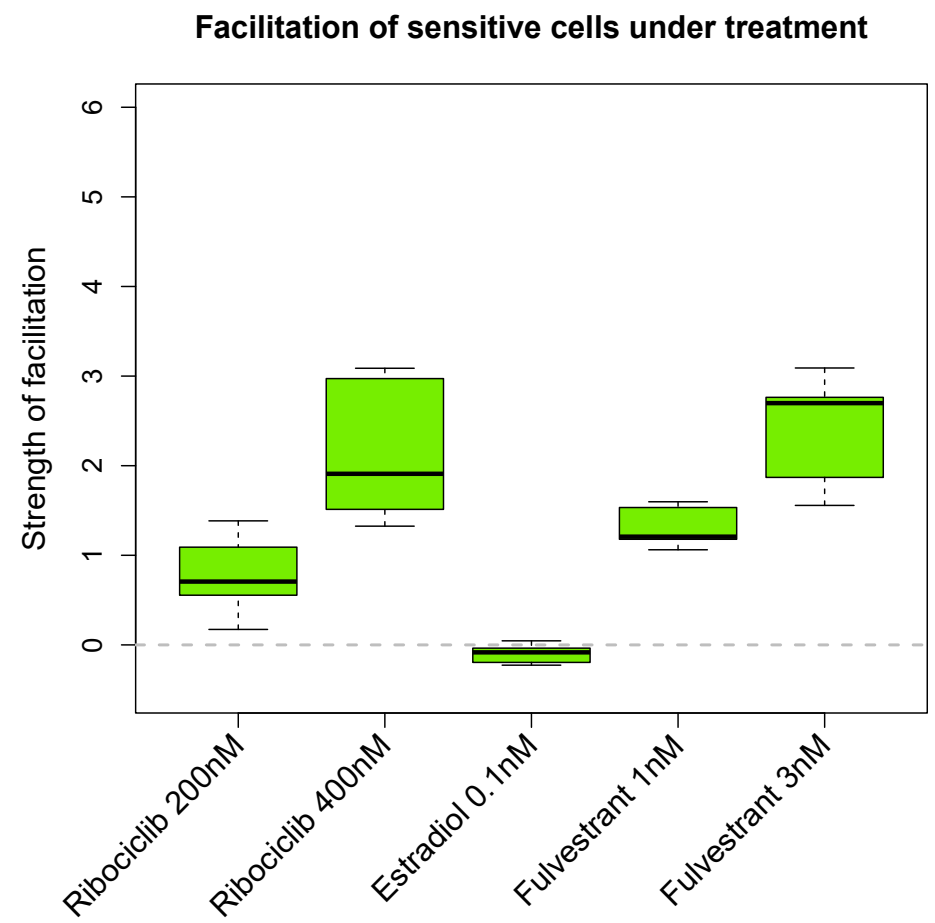
Facilitation of sensitive cells under treatment
Strength of facilitation
0
1
2
3
4
5
6
Ribociclib 200nM
Ribociclib 400nM
Estradiol 0.1nM
Fulvestrant 1nM
Fulvestrant 3nM

b

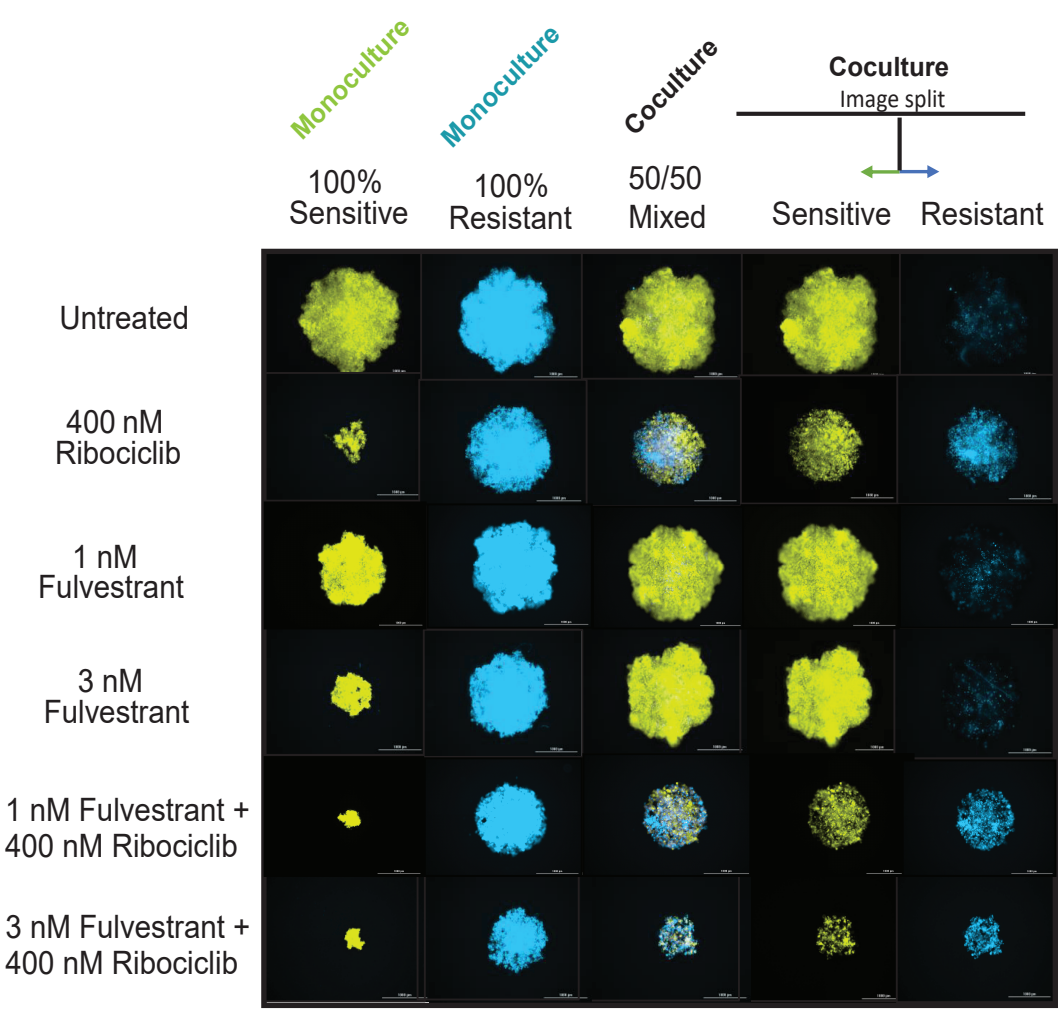
Fulvestrant
Monoculture
Monoculture
Coculture
Coculture
Image split
100% Sensitive
100% Resistant
50/50 Mixed
Sensitive
Resistant
Untreated
400 nM Ribociclib
1 nM Fulvestrant
3 nM Fulvestrant
1 nM Fulvestrant + 400 nM Ribociclib
3 nM Fulvestrant + 400 nM Ribociclib

d

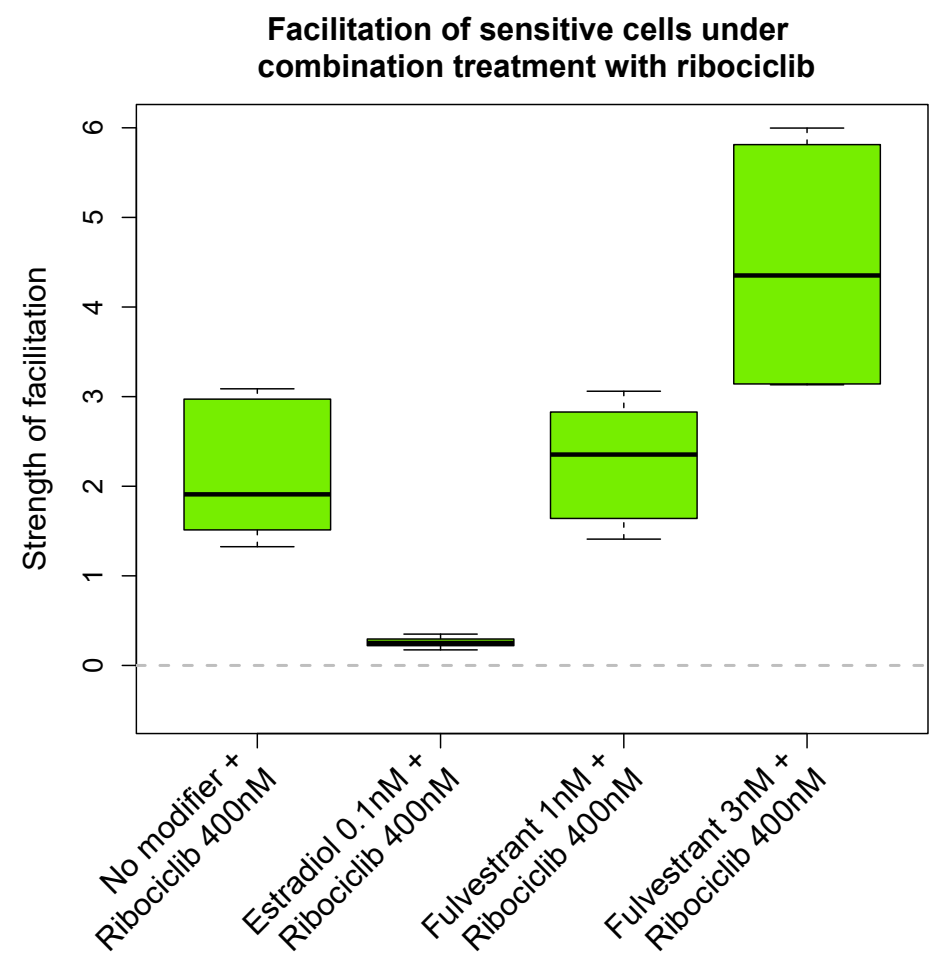
Facilitation of sensitive cells under combination treatment with ribociclib
Strength of facilitation
0
1
2
3
4
5
6
No modifier + Ribociclib 400nM
Estradiol 0.1nM + Ribociclib 400nM
Fulvestrant 1nM + Ribociclib 400nM
Fulvestrant 3nM + Ribociclib 400nM

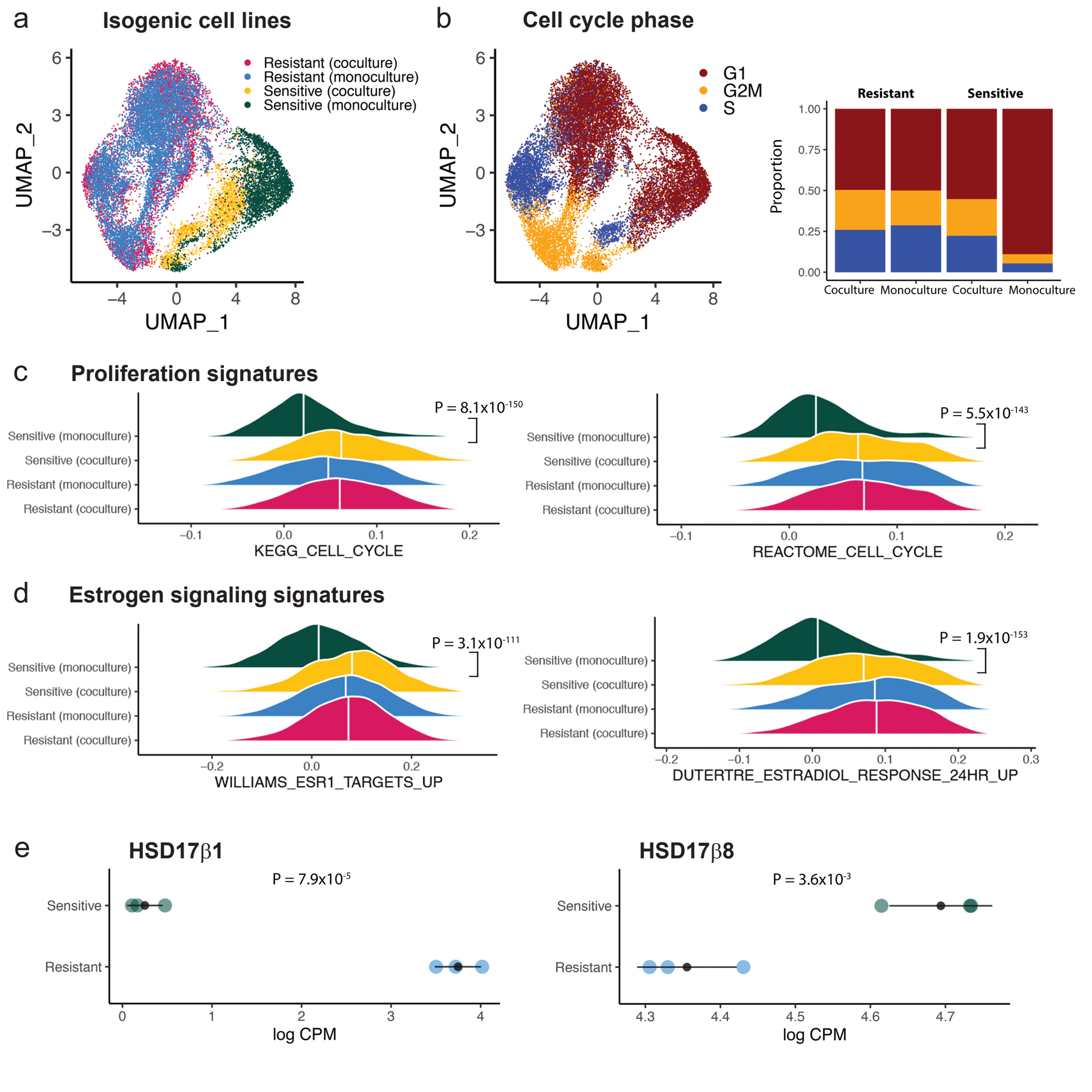
a
Isogenic cell lines
Resistant (coculture)
Resistant (monoculture)
Sensitive (coculture)
Sensitive (monoculture)
UMAP_2
UMAP_1
b
Cell cycle phase
G1
G2M
S
Resistant
Sensitive
Proportion
Coculture
Monoculture
Coculture
Monoculture
c
Proliferation signatures
P = 8.1x10-150
P = 5.5x10-143
Sensitive (monoculture)
Sensitive (coculture)
Resistant (monoculture)
Resistant (coculture)
KEGG_CELL_CYCLE
REACTOME_CELL_CYCLE
d
Estrogen signaling signatures
P = 3.1x10-111
P = 1.9x10-153
WILLIAMS_ESR1_TARGETS_UP
DUTERTRE_ESTRADIOL_RESPONSE_24HR_UP
e
HSD17β1
HSD17β8
P = 7.9x10-5
P = 3.6x10-3
Sensitive
Resistant
log CPM

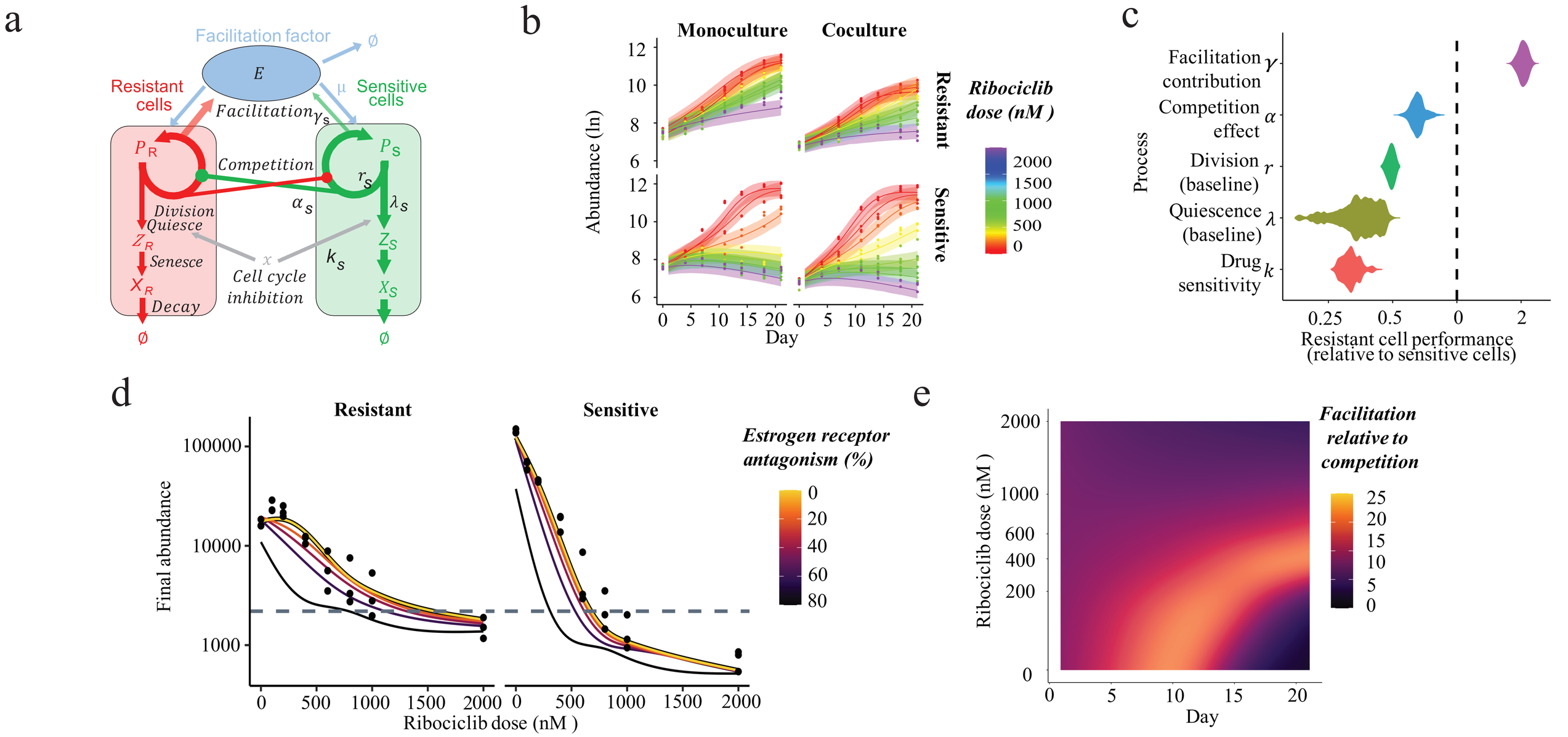
a
Facilitation factor
E
Resistant cells
Sensitive cells
Facilitation
Competition
Division
Quiesce
Senesce
Decay
Cell cycle inhibition
b
Monoculture
Coculture
Resistant
Sensitive
Abundance (ln)
Day
Ribociclib dose (nM)
2000
1500
1000
500
0
c
Facilitation contribution
Competition effect
Division (baseline)
Quiescence (baseline)
Drug sensitivity
Process
Resistant cell performance (relative to sensitive cells)
d
Resistant
Sensitive
Final abundance
Ribociclib dose (nM)
Estrogen receptor antagonism (%)
e
Ribociclib dose (nM)
Day
Facilitation relative to competition